Materials Advances

REVIEW

View Article Online
View Journal | View Issue

Cite this: *Mater. Adv.*, 2025, **6**, 2753

Croconic acid-based compounds: synthesis, structural characteristics, properties and applications of an intriguing class of functional organic materials

Maria Montrone,[ab] Umberto Berardi,*[c] Antonio Cardone *[d] and Maria Annunziata M. Capozzi*[b]

The present review springs up from the demand for an overview on the scientific advances in croconic acid-based materials and their potential technological applications. Modern technological challenges in the biomedical and energy fields share the common need for the use of environmentally friendly materials and devices that are safe for humans. Croconic acid-based compounds are an interesting class of functional organic materials of great potential since they combine intrinsic biocompatibility with chemico-physical properties that are very attractive for a number of applications, including in the biomedical sector, *i.e.*, theranostics; energy field, *i.e.*, energy conversion, energy storage and energy saving; and sensing field. Despite the high potential, to date, only few reviews covering specific aspects such as synthesis or, mainly, biomedical applications are available in the literature, while reviews summarizing all investigations performed on this intriguing class of organic materials, from their design to application, are lacking. Through an overview of synthetic approaches, basic structural characteristics, chemico-physical properties and applications, the present review aims to extensively analyse the research advances and the role played by such functional organic materials, with the hope of stimulating new insights for future perspectives.

Received 7th October 2024,
Accepted 8th March 2025

DOI: 10.1039/d4ma01006j

rsc.li/materials-advances

1. Introduction

In the ever-evolving landscape of materials science, the search for innovative and efficient materials to address the urgent challenges of technological and energy applications has led researchers to explore unconventional approaches. In this context, functional organic materials have been playing a key role in recent years, continuously gaining ground compared to their inorganic counterparts in electronic and photonic applications. The interest for organic materials lies in important advantages such as simple processing, low-cost manufacturing, light weight, high molecular versatility, and easy modulation of chemico-physical properties. Croconic acid-based compounds are a class of functional organic materials with intriguing electronic properties, strictly correlated with their conjugated molecular structure containing the croconate ring. They are reported in the literature both as croconaines or croconaine dyes and as croconate derivatives, being prepared by the condensation reaction of croconic acid with mainly electronic-donating units or, in rarer cases, electronic-acceptor units. In this review, we use the term croconaines (CRs) including the croconate derivatives. CRs[1] exhibit intense π–π* transitions, allowing optical absorption in the NIR region, which for a long time was attributed to the classical donor–acceptor charge transfer between the electron-donor substituents and the central croconic ring. Later, theoretical and experimental studies demonstrated that the NIR-absorption capability is a result of the biradical character of this class of molecules. As evidence of the key role of these aspects in defining properties and potential application of CRs, we discuss the most significant details in the subsequent section ''Structural aspects''. Features such as highly tuneable absorption spectra, with absorption peaks spanning from the visible to the near-infrared (NIR) region, high molar extinction coefficients (in the order of 10^4–10^5 L mol^{-1} cm^{-1}), and synthetic flexibility make CRs suitable materials for a lot of interesting applications, such as in organic photovoltaics,[2–6] photodynamic and photothermal

[a] *DEI, Polytechnic of Bari, Via Orabona 4, 70125, Bari, Italy. E-mail: m.montrone3@phd.poliba.it*
[b] *Department of Chemistry, University of Bari ''Aldo Moro'', Via Orabona, 4, 70125, Bari, Italy. E-mail: maria.capozzi@uniba.it*
[c] *Department of Architectural Science, Toronto Metropolitan University, 350 Victoria Street, Toronto, M5B 2D3, ON, Canada. E-mail: uberardi@torontomu.ca*
[d] *Institute of Chemistry of OrganoMetallic Compounds-ICCOM of Bari, Italian National Council of Research-CNR, Via Orabona, 4, 70125 Bari, Italy. E-mail: antonio.cardone@cnr.it, cardone@ba.iccom.cnr.it*

therapy,[7–20] and molecular or ionic sensors.[21–29] Over the past decade, the CR research landscape has witnessed a notable increase in interest, as reflected in the growing number of publications dedicated to unraveling the properties for harnessing the potential of these compounds. From 1970 to 2010, only a handful of publications, mostly patents, were delved into the exploration of CRs and their applications. Later, the number of documents or patents on CRs has multiplied, signifying an accelerating pace of discovery and growing recognition of their relevance in the framework of functional organic materials. To date, a limited number of reviews have been published, most of them surveying different classes of organic materials, including CRs, focused on some aspects and specific applications,[12,14,30–33] and only three reviews surveying exclusively CRs, two of which focused on CRs for biomedical applications[10,11] and one focused mainly on synthetic aspects.[1] In the first review, Fabian *et al.*[30] revised CRs within a wide variety of organic compounds with a diradicaloid character, in which there is a very small energy difference between the lowest energy electronic states. By proper structural modification, these types of molecules can be stabilized in a singlet form which absorbs at long wavelengths. In the same year, Emmelius *et al.*[31] revised materials for optical data storage, citing CRs within a class of methine-based dyes, in which the introduction of a cyclic unit into the methine group can be exploited as a tool to reduce the LUMO and then promote a bathochromic shift of the absorption maximum of dyes. In almost 30 years, from 1989 to 2018, no reviews were published on CRs. In 2018, two reviews were published on molecular photoacoustic contrast agents[32] and organic molecule-based photothermal agents[33] for biomedical applications. At first,[32] several types of organic dyes as photoacoustic agents for photoacoustic imaging were reviewed, with a very little space dedicated to CRs within a paragraph mainly focused to squaraines (pseudo-oxocarbon homologous with cyclobutene ring). Later,[33] a large number of organic molecules with photothermal properties for application in photothermal therapies for cancer were surveyed. In this review, only three papers reporting the results of investigation of two different CR dyes, in CR-rotaxane complexes, were selected. Later, in 2020[12] and 2021[14] two reviews were published, always focused on the recent development of photothermal agents for disease treatment. Once again, both these reviews marginally surveyed CRs, reporting the results of investigation on the same two CRs of previous reviews. In 2017, for the first time, a review entirely dedicated to CRs was published, retracing the history since 1970 and focusing the synthesis and structures up to that year.[1] The review also reported some crystallographic and spectroscopic (range of absorption) data. More recently, in 2020[10] and 2023,[11] two reviews entirely dedicated to CRs and focused on the recent advances in CR dyes for bioimaging and theranostics were published. These reviews surveyed many CR structures and their potential in photothermal therapy, photoacoustic imaging, phototheranostics and multimodal treatment aimed at clinical translation perspectives. Concurrently with our work, in 2024,[34] another review has been reported, also focused on CRs for bioimaging, therapy and metal detection. In line with the growing interest in croconic acid-based materials, with the aim to filling the gap of the lack of an overview exclusively dedicated to this class of materials, covering all chemico-physical properties and applications investigated, the present review wants to provide such a type of contribution, analyzing the most representative papers to date, focused on croconic acid-based materials, mainly CRs, and surveying the main synthesized chemical structures, structural aspects, chemico-physical properties and applications. We hope to give readers useful indications and stimuli for future development involving this attractive class of functional organic materials.

2. Structural aspects

Croconic acid-based compounds in general, and CRs in particular, are an important class of organic materials based on the croconic acid unit (Scheme 1) that have been known for more than 150 years and to which a lot of papers have been dedicated in the past few years.[1,35]

The croconate anion, with the general formula of $(C_5O_5)^{2-}$, possesses interesting structural features such as high symmetry, cyclic planar structure, extensive π-electron delocalization, and aromatic character.[36] Moreover, the croconate anion displays good acceptor ability and its crystal lattice is stabilized by strong H-bonds and π–π interactions between adjacent layers, giving rise to extended supramolecular 3D structures. These are key characteristics to determine and address optical and electric properties in solid-state material chemistry. Despite their appealing features, compared with squaraines, CRs have not received the same attention, even though they exhibit higher photostability, higher synthetic yields, and stronger absorption shifted at longer wavelengths, revealing even higher potential. Generally, CRs are a class of functional organic materials consisting of 2 donor moieties connected to 2 and 5 positions of the central 5-member croconate ring, with a donor–acceptor–donor (D–A–D) structure.[37–39] The D–A–D structure ensures extended π-conjugation, which gives these materials semiconductor properties. By an accurate choice of the donor units, it is possible to modulate the HOMO and LUMO energy levels and then the band gap, addressing electrical and optical properties for specific applications. CRs show features such as high absorption extinction coefficient, high photostability, and narrow and intense absorption bands in the NIR region (absorption at a wavelength longer than 1100 nm).[40,41] The NIR absorption capability of CRs, initially attributed to the strong donor–acceptor molecular charge transfer, has been recently definitively attributed to the biradical character (Scheme 2).[38,42]

The electronic structure of the molecule can be considered as the result of two resonance contributions, that of the

Scheme 1 Croconic acid (left) and croconate anion (right).

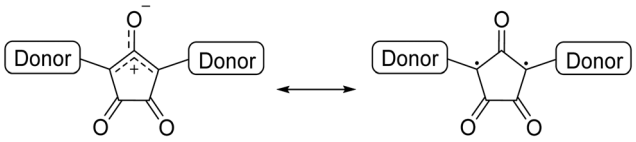

Scheme 2 Resonance structures in CRs: mesoionic (left) and biradical (right) forms.

mesoionic form and that of the biradical form. These two electroisomers are in equilibrium; but by acting on the geometry and substitutions of the conjugated skeleton, the structure can be stabilized either in the mesoionic form or in the biradical form. Computational studies demonstrate that the CRs exhibit strong tendency towards the biradical form.[43] The small band gap is also a feature favouring the formation of open-shell singlet or triplet states and, therefore, the enhancement of the diradical character. Since the energies of the singlet and triplet states are related to the biradical character of the ground state, which may be tuned by chemical structure modifications, the final properties of the molecule can be tuned by a proper chemical design.[44] The first study on the biradical character of CRs date from the 1989, when Fabian and Zahradnik[30] classified some organic compounds as diradicaloid dyes. They pointed out that the diradical nature of these compounds shifts the absorption towards longer wavelengths and suggested representing their diradical nature by non-Kekulé structures (Scheme 3).

More recently, Maeda *et al.*[45] have investigated the CRs CR2a and CR2b (Scheme 4 and Table 1) by ^{1}H-NMR, ESR and X-ray crystallography analyses, and DFT calculations provided experimental proof of the diradical character of CRs, in agreement with what was theorized by Fabian and Zahradnik.[30] The ESR spectra of CR2a and CR2b and ^{1}H NMR spectra of CR2b at different temperatures are reported in Fig. 1 as the spectroscopic evidence of the singlet and triplet formation of diradicals in CRs.

In a singlet diradicaloid molecule, the two antiparallel electrons are partially coupled but not fully coupled in the ground state. Their coupling degree can be expressed by using the diradical character y_0, which can be experimentally determined using the following equation:

$$y_0 = 1 - \sqrt{1 - (E_{OPA} - E_T/E_{TPA})^2}$$

where E_{OPA} is the energy level of the one-photon absorption-allowed (OPA) excited state obtained from the OPA peak, E_{TPA} is the energy level of the two-photon absorption-allowed (TPA) excited state obtained from the sharp TPA peak, and E_T is the energy level of the triplet state. It ranges between 0 and 1, where y_0 = 0 and 1 represent closed-shell and open-shell electronic structures, respectively (Fig. 2).

Moreover, X-ray crystallographic analysis of the single crystal also revealed that CR2b adopts a highly planar *cis* conformation. In 2018, López-Carballeira *et al.*[44] defined the diradical character y_0 of a series of squaraines and CRs. Higher values of y_0 were observed for the CR dyes (between 0.18 and 0.72). This was ascribed to lower HOMO–LUMO gaps as well as to higher values of the angle of the oxyallyl subgroup, as larger angles stabilize the LUMO and destabilize the HOMO orbitals, reducing the HOMO–LUMO gap. It is worthy of mention that the importance of the donor units for the diradical character. For example, the highest diradical characters are calculated

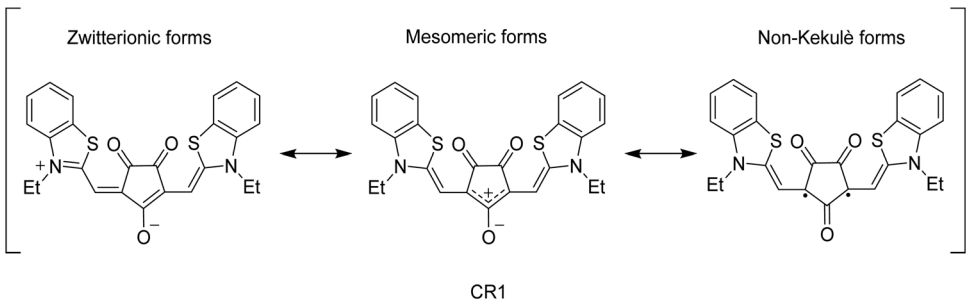

Scheme 3 Resonance structures including zwitterionic, mesomeric, and non-Kekulé forms of CRs constructed according to the hypotheses presented in ref. 26. CR1 reported in ref. 30 was used as the reference molecule to represent the resonance structures.

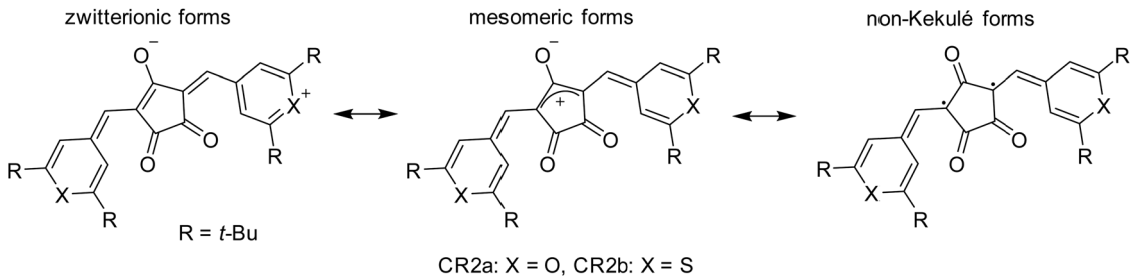

Scheme 4 Resonance structures including zwitterionic, mesomeric, and non-Kekulé forms of CR2a and CR2b (from ref. 45).

Table 1 Structure and synthetic conditions of CRs, with CR19 and CR20 being the patented structures

Dye structure	Acceptor	Donor	Solvent reaction	Ref.
CR2		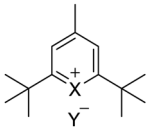 Y: CF_3SO_3, PF_6; X: O, S; CR2: a, b	Pyridine/MeOH	44 46
CR18		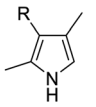 CR18: a H; b C_2H_5; c CH_3; d $CO_2C_2H_5$	EtOH	47
CR19		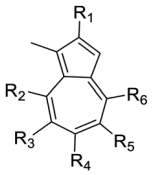	*n*-BuOH/benzene	48 49 50
CR20	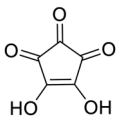	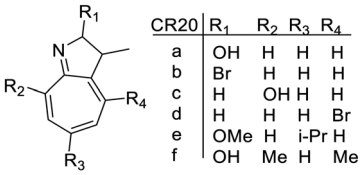 CR20: a OH H H H; b Br H H H; c H OH H H; d H H H Br; e OMe H i-Pr H; f OH Me H Me	*n*-BuOH/benzene	51
CR21		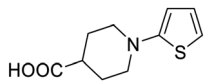	Toluene/*n*-BuOH	24
CR5		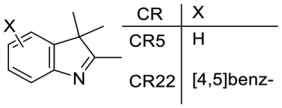 CR: CR5 H; CR22 [4,5]benz-	Solvent free: – IR-light	18,52
CR22			– Conventional thermal activation – Mechanical milling activation	
CR23		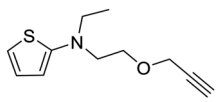	Toluene/*n*-BuOH	53
CR24		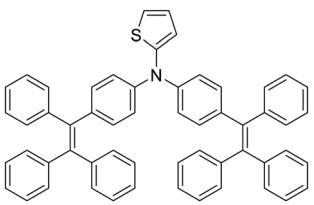	Toluene/*n*-BuOH	16

for CR3a–c and CR4 (Scheme 5), with y_0 values between 0.63 and 0.72. In CR3a–c, the resonant form of the closed-shell singlet involves a positively charged heteroatom (O, S or Se), which destabilizes the mesoionic form, making it more difficult to integrate a positive charge and favouring the delocalization of the spin density along the substituents, leaving the four- or five-membered rings unchanged. It is also remarkable that the high diradical character of CR4 (0.72) due to the large delocalization of the unpaired electrons in the croconate moieties.

The singlet diradicaloids exhibit intriguing functionalities such as electric conductivity, optical nonlinearity including TPA, and singlet fission.[44,45,54,55] In 2016, for the first time, Punzi *et al.*[56] explored the charge transport properties of some CR dyes by structural investigation both in solution and in the solid state. X-ray analysis confirmed that molecules are essentially planar with the π system delocalized over the whole molecule. It also revealed a solid-state packing characterized by parallel sheets linked by electrostatic and π–π stacking interactions, resulting in extended π-conjugation favouring charge transport for both electrons and holes. However, this is the first work reporting the crystal structures of CRs, obtained for CR5 and CR6, by the single-crystal X-ray diffraction (SCXRD) technique (Scheme 6 and Fig. 3).

In the present case, as well as, in general, for symmetric CRs, three configurations are possible for both CRs (the structure of CR5 is shown as the example, Fig. 3(a)), two symmetric with the N atoms on the same side of the molecule (*cis*1 and *cis*2) and

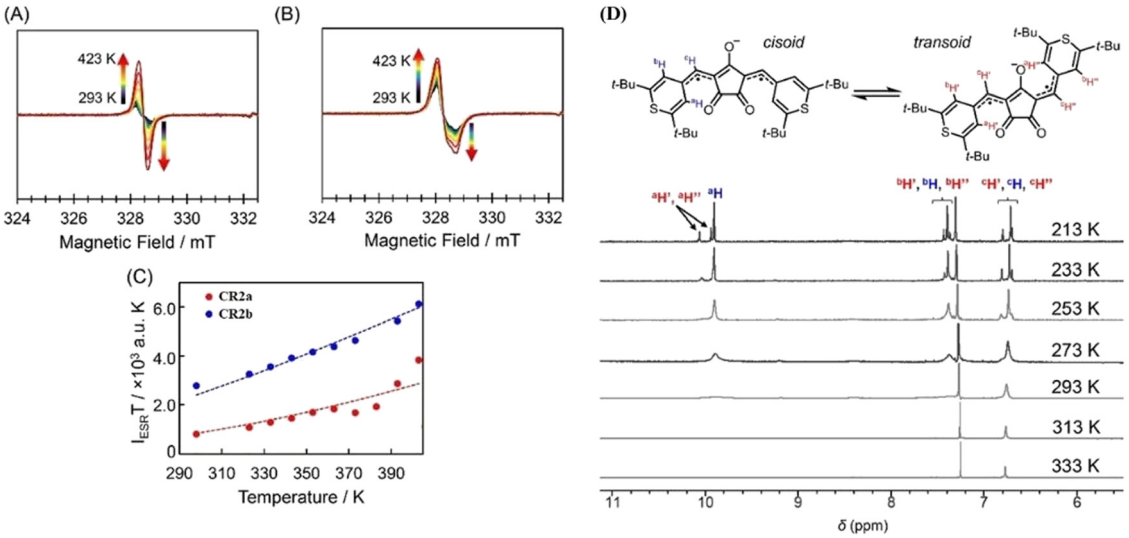

Fig. 1 ESR spectra of the powder samples CR2a (A, g = 2.003) and CR2b (B, g = 2.006) and temperature–$I_{ESR}T$ plots based on the ESR data of CR2a (red) and CR2b (blue); the dotted lines are the fitted plots constructed using the Bleaney–Bowers equation (C). Variable temperature ^{1}H-NMR spectra ($CDCl_3$, 213–333 K) of CR2b (D). Reproduced with permission from ref. 45. Copyright 2015, the American Chemical Society.

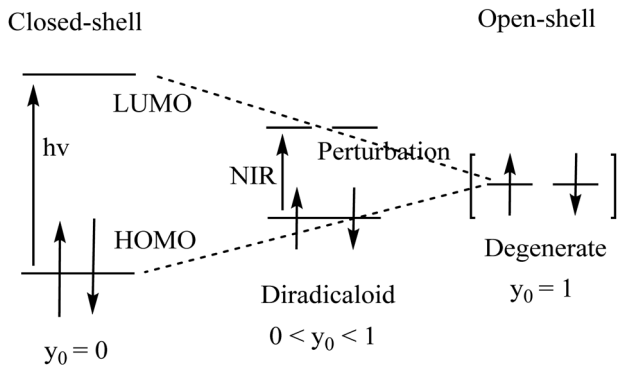

Fig. 2 Relationship between transition energy and open-shell character. y_0 indicates the diradical character. Reproduced with permission from ref. 45. Copyright 2015, the American Chemical Society.

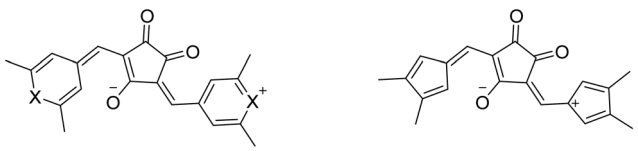

Scheme 5 Structures of CR3a–c and CR4 and their related y_0 values.

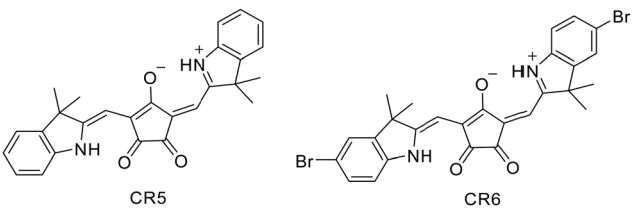

Scheme 6 Structures of CR5 and CR6.

one asymmetric with the N atoms opposite with respect to the molecule barycentre (*trans*). Each conformer is stabilized by two N–H···O=C H-bonds, involving two symmetric C=O groups in the *cis*1 conformation, the same C=O group in the *cis*2 conformation and two different carbonyl oxygens in the *trans* conformation. The *trans* conformation results in the most stable isomer and also the molecular arrangement found in all the crystals isolated (the crystal structure of CR6 is shown as the example, Fig. 3(b)).

Different CRs will have different stabilizing interactions in the three conformations, yielding to a different stability of the three isomers, depending on the chemical structure of the molecule. For the purpose of the present review, we chose to depict the CRs in the graphical diagrams in the *trans* or *cis* configuration, keeping the structure reported by the authors in the literature, taking into account that the determination of the configuration, not just theoretical calculations, has only recently been reported in a few scientific papers, mainly in the related Supporting Informations. [53,57–60]

3. Synthetic aspects

Generally, CRs are characterized by a short π-conjugated backbone containing an oxyallyl subgroup and are easy to synthesize *via* a straightforward condensation reaction. In addition, they are able to easily undergo chemico-structural variations that allow tuning their chemico-physical properties, addressing them for various applications. To date, many CRs have been synthesized, mainly with a symmetric structure and in few

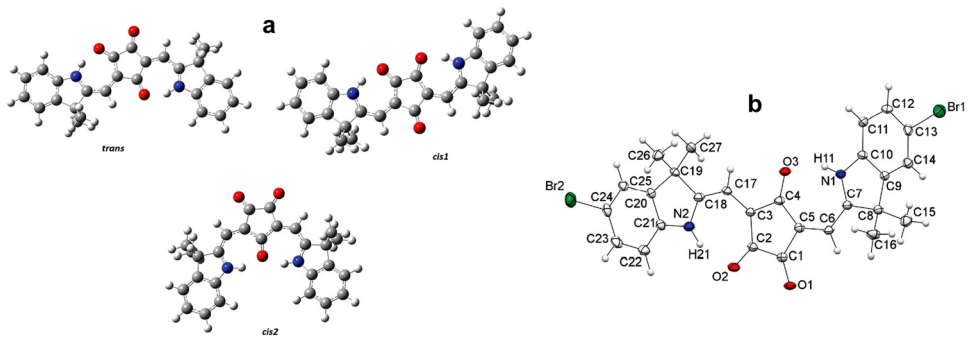

Fig. 3 (a) Most stable conformational isomers of CR5 and (b) X-ray structure of CR6. Reproduced with permission from ref. 56. Copyright 2016, the Royal Society of Chemistry.

cases with a nonsymmetric structure, by connecting to the croconate ring two identical or different donor units, respectively. The first synthesis of CRs was reported in a German patent in 1970 by Agfa-Gevaert,[61] which was subsequently divided in two US patents.[62,63] In these patents, the synthesis of new CRs was reported (CR1, CR7–17), based on the condensation reaction of croconic acid with different electron donor reagents, at room temperature using different solvents, *i.e.* methanol/pyridine and triethylamine, pyridine/triethylamine or methanol/pyridine mixtures (Scheme 7).

However, this first report has not achieved the same success in the subsequent scientific literature as the papers on the squaraines, and hence, the synthesis of new CRs was often reported together with that of squaraines or other pseudo-oxocarbon compounds (*i.e.* rhodizonaines and/or deltaines).[65–67] In 1973, Treibs *et al.*[47] reported the synthesis of four pyrrolyl CRs (CR18a–d, Table 1, $\lambda_{max} > 690$ nm) together with the synthesis of five pyrrolyl rhodizonaines, using ethanol as the solvent, at different temperatures. In a US patent in 1985,[48] followed up in 1988[49] by Canon Kabushiki Kaisha, the synthesis of azulenyl CRs (CR19, Table 1) using butanol/benzene as the solvent was reported for the first time. In 1989, Yasui *et al.*[64] reported the synthesis of CRs of type CR1 and CR7-10, referring to the Agfa-Gevaert patent[61] from 1970 for synthesis details. Following, a US patent from 1989 by Fuji Photo Film[51] and a US patent by Canon Kabushiki Kaisha from 1990[50] reported the synthesis of six aza-azulenyl CRs (CR20a–f, Table 1) and five azulenyl CRs (CR19, Table 1), respectively. Since 1970, a number of CRs have been successfully prepared by introducing various donor units such as quinuclidine, indole, thiophene, benzothiazole, benzooxazole, and aniline derivatives.[1,10] They were prepared following several synthesis protocols, *i.e.*, using different alcohols (MeOH, EtOH or BuOH) and/or different organic bases (pyridine/triethylamine mixtures, or quinoline), or using solvent mixtures such as butanol/benzene under reflux[68] or butanol/toluene in an inert atmosphere (N_2) or in air (CR21, Tables 1 and 2).[24] Good to high reaction yields (45–95%) were reported for CRs prepared by refluxing butanol/toluene mixtures for a short reaction time ($\leq$2 h), both in an inert atmosphere (N_2,[56] Ar[57,58]) and in air,[69,70] without azeotropic water removal. From 1990 to 2018, only symmetric CRs were reported in the literature.

In 2018, Capozzi *et al.*[59] synthesized new croconic acid derivatives: semicroconaines and nonsymmetric CRs. Semicroconaines

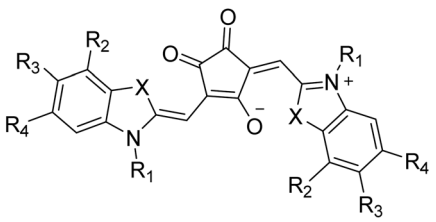

CR1 X = S, $R_1 = CH_3CH_2$, $R_2 = R_3 = R_4 = H$
CR7, X = S, $R_1 = CH_3CH_2$, $R_2 = Cl$, $R_3 = R_4 = H$
CR8, X = S, $R_1 = CH_3$, $R_3 = OCH_3$, $R_2 = R_4 = H$
CR9, X = S, $R_1 = CH_3CH_2$, $R_2 = R_3 = H$, $R_4 = CH_3$
CR10, X = S, $R_1 = (CH_2)SO_3H{\cdot}C_5H_5N$, $R_2 = R_3 = R_4 = H$
CR11, X = S, $R_1 = (CH_2)SO_3H{\cdot}C_5H_5N$, $R_4 = CH_3$, $R_2 = R_3 = H$
CR12, X = S, $R_1 = (CH_2)COOH$, $R_4 = Ph$, $R_2 = R_3 = H$
CR13, X = Se, $R_1 = CH_3$, $R_4 = OCH_3$, $R_2 = R_3 = H$
CR14, X = Se, $R_1 = (CH_2)SO_3H{\cdot}C_5H_5N$, $R_2 = H$, $R_3 = R_4 = CH_3$
CR15, X = $C(CH_3)_2$, $R_1 = CH_3$, $R_3 = Cl$, $R_2 = R_4 = H$

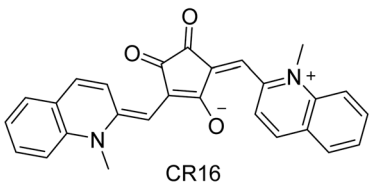

CR16

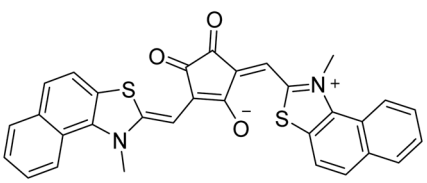

CR17

Scheme 7 CRs with symmetric structures. Patented structures ref. 62 and 63. CR1 was reported in ref. 30. CR8 was reported in ref. 38, 43 and44. CR10 was reported in ref. 64. CR16 was reported in ref. 18, 23, 38, 43 and64.

Table 2 Fluorescence of CRs

Dye structure	Excitation wavelength (nm)	Fluorescence (nm)	Ref.
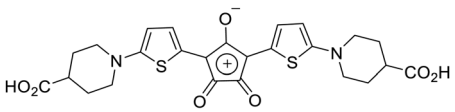 CR21	808	1000–1400	71
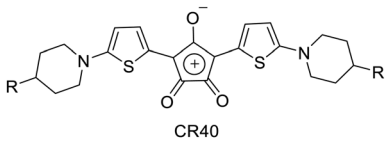 CR40	780	815	15
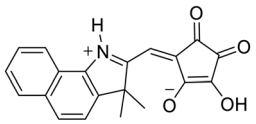 S-CR1	563 (H_2O) 574 (MeOH) 560 (CH_3CN) 552 (DCM)	639 (H_2O) 631 (MeOH) 616 (CH_3CN) 613 (DCM)	59
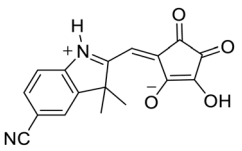 S-CR2	564 (H_2O) 555 (MeOH) 541 (CH_3CN) 516 (DCM)	599 (H_2O) 593 (MeOH) 598 (CH_3CN) 601 (DCM)	59

(S-CRs) were selectively prepared *via* a base-free condensation reaction between croconic acid and methylene active-based aromatic heterocyclic compounds with a rigorous control of reaction conditions (optimized reaction conditions for S-CR1: yield = 86%, solvent = H_2O/acetone, time = 4 days, temperature = 50 °C). The nonsymmetric CRs CR25a–c were synthesized in good yields, starting from the semicroconaine S-CR1, submitted to a second condensation reaction, as reported in Scheme 8.

The new pool of CRs was investigated by absorption and emission spectroscopy in different solvents, ^{1}H NMR spectroscopy and theoretical calculations. In 2021, the same research group, reported the successful application of the emerging synthetic protocols based on solvent-free mechanochemical (ball-milling) and IR irradiation conditions to the preparation of indolenine-based CRs (CR5 and CR22, Table 1; CR25a, Scheme 8).[52] Their study showed that the use of ball-milling

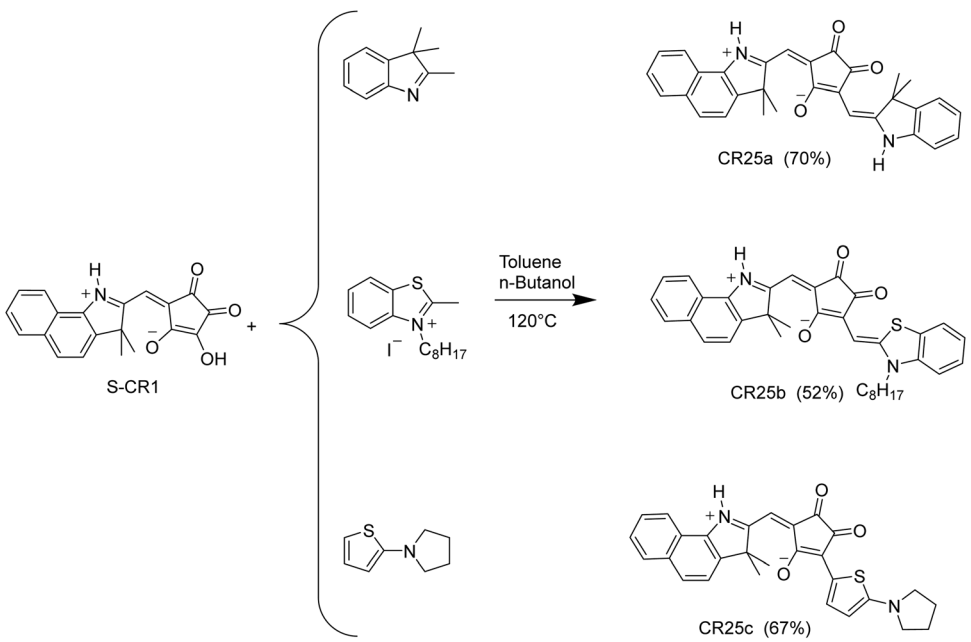

Scheme 8 CRs with a non-symmetric structure.

(yield 64–67%, 3 h) was a valid alternative to the conventional heating (yield 17–62%, 1–2 h) under solvent-free conditions for the synthesis of CRs. Furthermore, irradiation with an IR lamp promotes the condensation reactions, even under solvent-free conditions, with considerable shorter reaction times (yield 43–64%, 90 s–1 h) and reduced energy consumption. In 2013, the first permanently interlocked CR-rotaxane systems were successfully prepared by Smith *et al.*[57] using stoppering and clipping-based synthetic strategies. The new croconaine-rotaxane (CR26-rotaxane, Scheme 9) and pseudorotaxane architectures showed interesting properties such as efficient photothermal performance in both organic and aqueous environments.

From 2013 to 2019, Smith *et al.*[53,60] continued research on CRs, by synthesizing new NIR-absorbing CRs with two thienothiophene flanking units, which were converted into rotaxane, *via* a ''clicked capping'' reaction. Polycroconaines (P-CR27a and P-CR27b Scheme 10) were first reported by Havinga *et al.* in 1992,[72] who used a condensation reaction carried out in a higher saturated alcohol as the synthetic protocol, at reflux and with inorganic acid (HCl, H_2SO_4) or quinoline as the catalyst. Later, in 1995, Havinga *et al.*[73] reported a water-soluble polycroconaine P-CR28 with the same conjugated structure of P-CR27 (Scheme 10), obtained by refluxing the two starting reagents in *n*-butanol for 20 hours, while removing water by means of azeotropic distillation. The first patent covering polycroconaines appeared in 1994,[74] although the synthetic details were not stated. The polycroconaines are stable in air at room temperature and can be heated up to 300 °C in air without any observable degradation. The chloroform solutions, however, deteriorate upon standing in air and daylight. Under these circumstances, the polymers degrade to oligomers. Polycroconaines are semiconductors with a small band gap down to 0.5 eV (P-CR29, Scheme 10).[75]

In 2022, Taylor *et al.*[67] reported the synthesis of new porous organic polymers (POPs), *via* a polycondensation reaction between

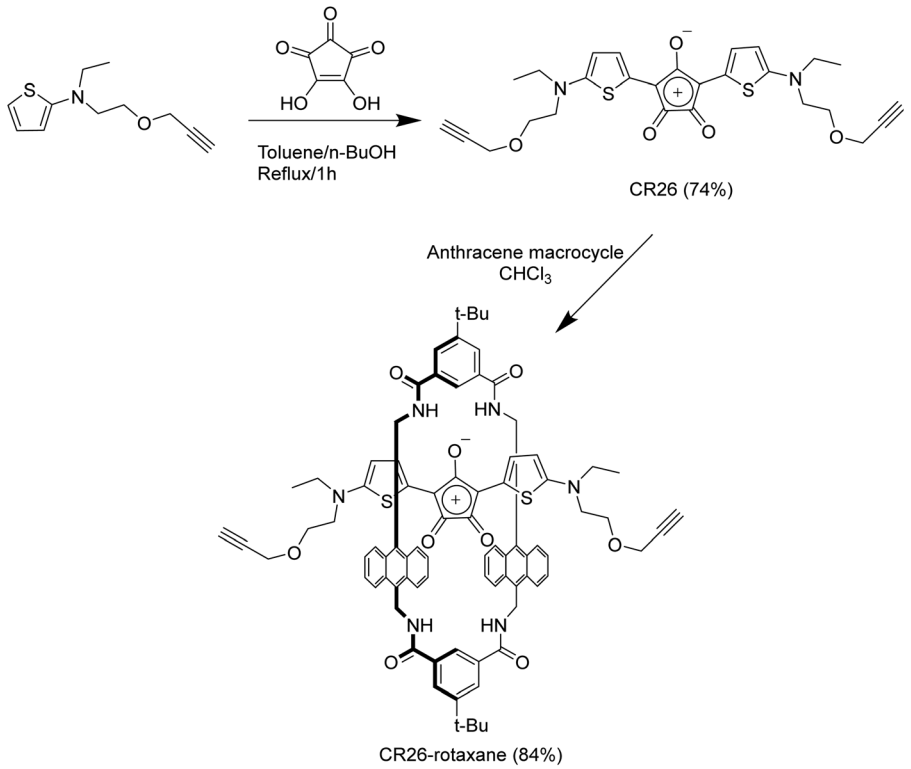

Scheme 9 Croconaine-rotaxane system.

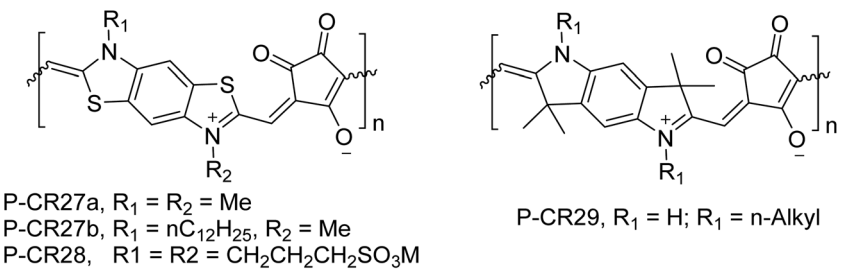

Scheme 10 Polycroconaines P-CR27–29.

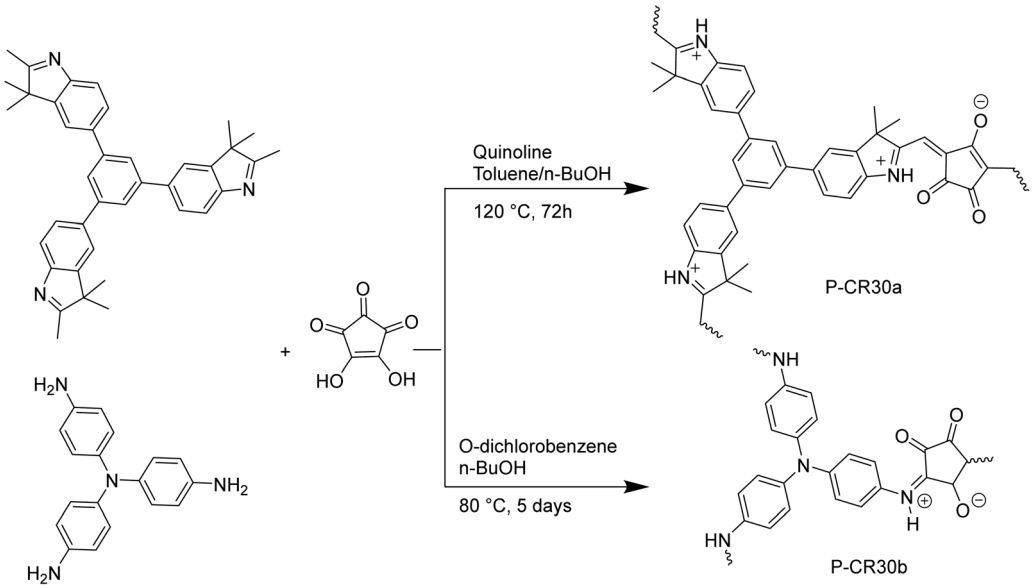

Scheme 11 Synthesis of polycroconaines P-CR30a,b.

a tritopic indole-based monomer and croconic/squaric/rhodizonic acid. The reactions were performed using quinoline as the base-catalyst and a butanol/toluene mixture as the solvent, in a nitrogen atmosphere at 120 °C for 72 h (Scheme 11, for the CR-based polymer only, P-CR30a). The POPs were isolated with excellent yields in the range of 85–97%. The CR-based polymer with zwitterionic structures was found to be a relatively weak proton conductor. Following this, in 2023, Enoch *et al.*[76] reported the synthesis of a new CR-based microporous polymer with a narrow band gap, *via* a polycondensation reaction between the triamino triphenyl amine (TPA) and croconic acid, in *o*-dichlorobenzene/*n*-butanol as the solvent, at 80 °C for 5 days (Scheme 11, P-CR30b). Comparing P-CR30b with the corresponding squaric acid congener polymer, they found superior optical, electronic and electrical properties for the croconic acid derivative.

Since 2021, four papers have been published, reporting the synthesis of new CR-based polymers for sensing applications. In 2021,[77] Yu *et al.* reported the synthesis of poly(4,4′-biphenylcroconate) (P-CR31a, Scheme 12), carried out by reacting croconic acid with 4,4′-biphenylenediamine, in acetonitrile at 125 °C for 12 h. The resulting polymer was investigated as an organic semiconductor gas sensor operating at high temperatures. In 2023, Zhou *et al.*[78] reported the synthesis of poly(1,5-diaminonaphthalene-croconaine) (P-CR31b, Scheme 12), carried out by reacting croconic acid with 1,5-diaminonaphtalene, in *o*-dichlorobenzene/*n*-BuOH at reflux for 13 h. The polymer was investigated as an ultra-sensitive NH_3 gas sensor in a core–shell composite system made of $Ti_3C_2T_x$ MXenes. Moreover, in 2023, Chen *et al.*[79] synthesized two new CR-based polymers, poly(1,5-diaminoanthraquinone-croconate) and poly(2,6-diaminoanthraquinone-croconate) (P-CR31c and P-CR31d, respectively in Scheme 12), by reacting croconic acid with 1,5-diaminoanthraquinone and 2,6-diaminoanthraquinone, respectively, in *n*-BuOH at 135 °C for 24 h. They were investigated as ion-in-conjugation polymer-based humidity sensors. In 2024, Wang *et al.*[80] reported the synthesis of the azo-spaced polymer poly(4,4′-azodianiline-croconamide) (P-CR31e, Scheme 12), carried out by reacting croconic acid with 4,4′-azodianiline, in methanol/tetrahydrofuran at 80 °C for 24 h. The polymer was investigated for gas sensing under humid conditions.

From early 2000, in line with the growing interest in nanomaterials, there has also been a development of the research towards the production of CR nanoparticles, prepared by different synthetic protocols. The first nanostructure was prepared by Smith *et al.*,[53] for which CR-doped silicate micelle nanoparticles were synthesized by a known procedure that first encapsulated hydrophobic dyes within Pluronic micelle cores and then formed permanent nanoparticles by silica deposition. Tang *et al.*[81] synthesized new self-assembled nanoparticles by polyethylene glycol (PEG)-conjugated CR starting from CR21 (Tables 1 and 2) (CR21-PEG-NPS). CR21-PEG was readily suspended in aqueous solutions and spontaneously self-assembled into well-defined and uniform nanostructures, with a size tunable by applying different molecular weights of PEG (PEG5K, M_w = 5 kDa; PEG2K, M_w = 2 kDa; PEG132, Fig. 4).

In 2021, Liu *et al.*,[82] using the same croconaine CR21, reacted with polyethylene glycol H_2N-PEG_{2000}-SH, prepared croconaine-modified polyethylene glycol CR21-PEG-SH, which was then functionalized by two different cancer-targeting peptides c(RADyC) or c(RGDyC) to yield CR21-PEG-RAD or CR21-PEG-RGD. These polymeric systems, characterized by the hydrophobic CR21 and the hydrophilic H_2N-PEG_{2000}-SH and c(RADyC) or c(RGDyC), can be easily self-assembled in nanoparticles by ultrasonication in deionized water. The resulting nanoparticles CR21-PEG-RAD@NPs and CR21-PEG-RGD@NPs were successfully investigated as highly efficient contrast agents for targeted optoacoustic imaging of murine brain tumors. In 2022, Liu *et al.*[16]

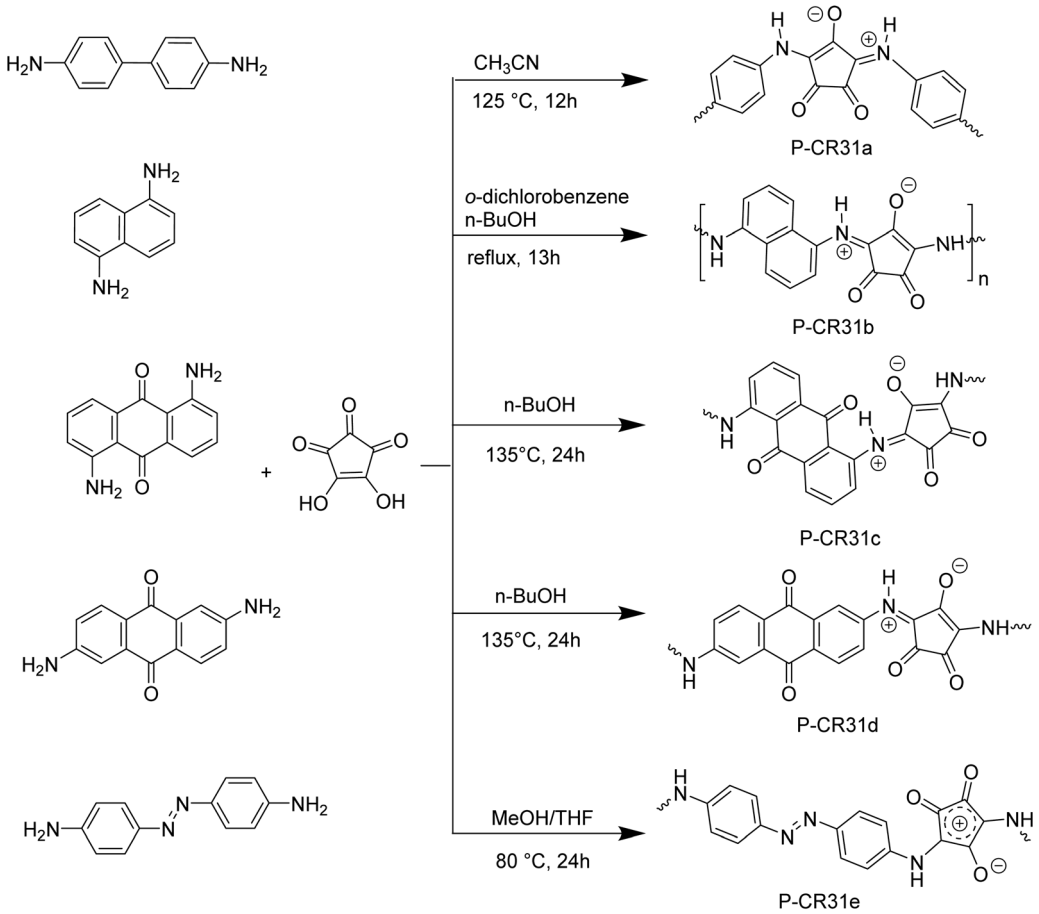

Scheme 12 Synthesis of P-CR31a–e.

reported multifunctional and water-soluble CR nanoparticles prepared by the nanoprecipitation method starting from CR24 (Table 1) and DSPE-PEG2000, which were first dissolved in THF, and then, the mixed solution was quickly injected in deionized water and a microtip probe sonicator was employed to sonicate the solution for 2 min, followed by removing the remaining THF using a rotary evaporator.

4. Chemico-physical properties

Croconic acid-based compounds display semiconducting properties, with absorption spanning from visible to NIR region (also with absorption at a wavelength longer than 1100 nm) and key features such as structural flexibility, high absorption capability, photostability, narrow and intense absorption bands. Furthermore, they show intriguing electro-optical, photo-acoustic and photo-thermal properties that can be exploited for the realization of high technology devices. A key aspect of CRs lies in the possibility to modulate their chemico-physical properties, including the solubility in organic and/or aqueous solvents, by the accurate design of the chemical structure and/or functionalization. In this review, we analyse the most intriguing chemico-physical properties of CRs, also in relation to potential applications.

4.1 Optical properties

4.1.1 Visible-NIR absorption. Visible-NIR absorbers are compounds capable of absorbing radiation with a wavelength between 400 and 1400 nm. This ability was one of the most studied early features of CRs. In 1992, in a worldwide patent by Polaroid Corporation, Telfer *et al.*[83] reported a new CR (CR34, Fig. 5) capable of absorbing in the NIR with high extinction coefficients.

They were obtained as a brown solid and a purplish solid, respectively, with absorption maxima above 900 nm. While in 1993,[69] CRs based on (2-thieny1) and (4-dialkylaminoaryl) (CR32 and CR33, Fig. 5) were reported, characterized by strong absorption bands in the NIR with λ_{max} in the range of 750–850 nm. In 2000,[46] four new CRs (CR2a,b and CR37a,b Fig. 5) were prepared starting from the pyrilium system and replacing the pyrilium O atom with S, Se or Te atoms. They showed absorption maxima in the range of 845–1080 nm, with a λ_{max} shifting toward a longer wavelength as the heteroatom size increased. In 2001, in a US patent,[84] the high NIR absorption capacity of CRs was exploited to improve the heating rate of a resin by adding two or more heating aids (one of these was a CR), which were chosen in order to promote broader and stronger absorbance in the NIR, with little or no increase in absorbance in the visible region of the spectrum. In 2003,[40,41]

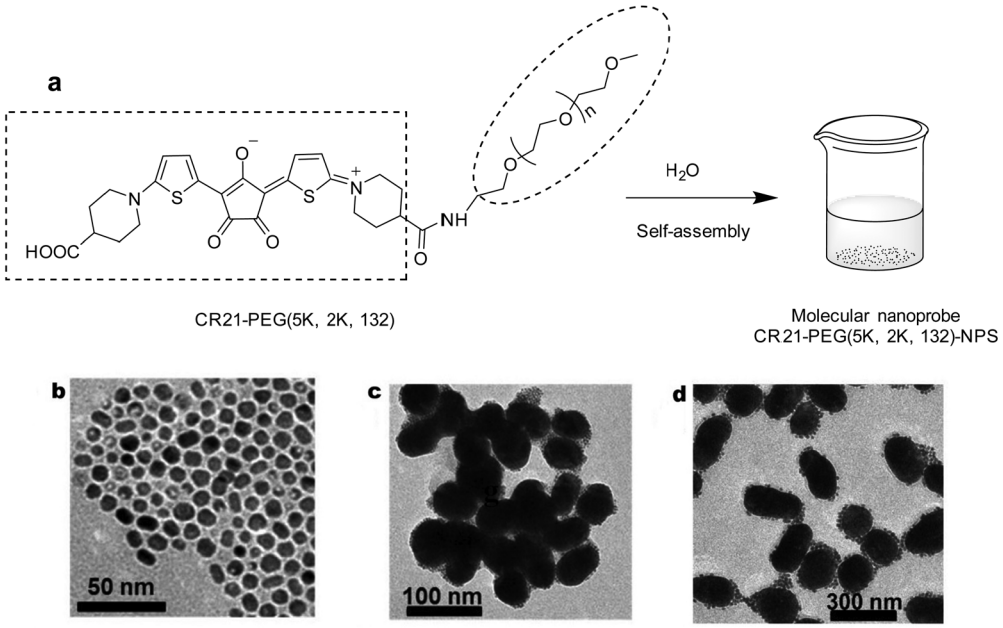

Fig. 4 (a) Schematic illustration of the preparation of CR21-PEG-NPS nanoparticles. (b)–(d) Transmission electron microscopy (TEM) images of CR21-PEG5K-NPS (0.15 mM) (b), CR21-PEG2K-NPS (0.15 mM) (c), and CR21-PEG132-NPS (0.15 mM) (d). Reproduced with permission from ref. 77. Copyright 2017, Elsevier.

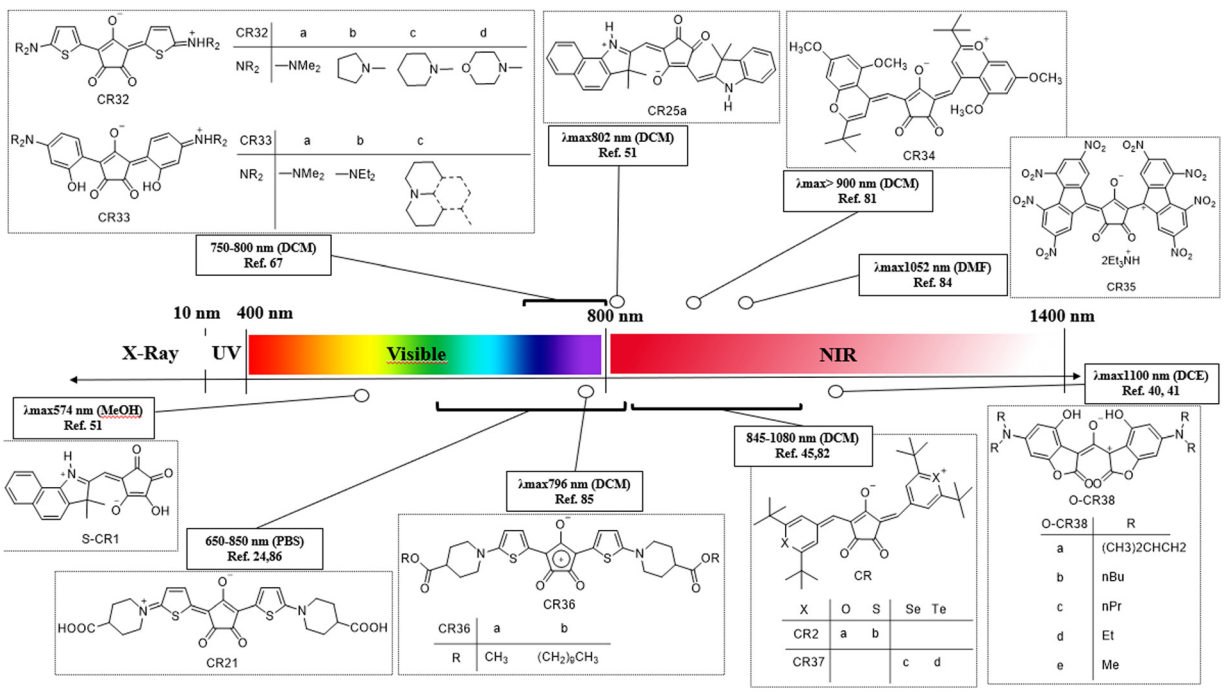

Fig. 5 Spectral absorption range of CRs.

CRs with absorption maxima at approximately 1100 nm, and features such as a relatively short backbone structure, good solubility in organic solvents ($ClCH_2H_2Cl$, $CHCl_3$, and THF) and high thermal stability were reported (O-CR38a–e, Scheme 13 and Fig. 5).

More recently, a squaraine and a CR (CR35, Fig. 5), obtained by reacting tetra-nitrofluorene with squaric acid and croconic acid, respectively, were synthesized and compared.[85] They represent a unique case in the history of squaraines/croconaines, as the squaraine showed the absorption at longer wavelengths than the CR (λ_{max} 1058 and 1052 nm, respectively, in DMF). Subsequently, Guo *et al.*[71] reported the first example of a calamitic mesogenic NIR-absorbing CR with λ_{max} = 796 nm (CR36b, Fig. 5). Nowadays, the NIR-absorbing capability of CRs is highly wanted

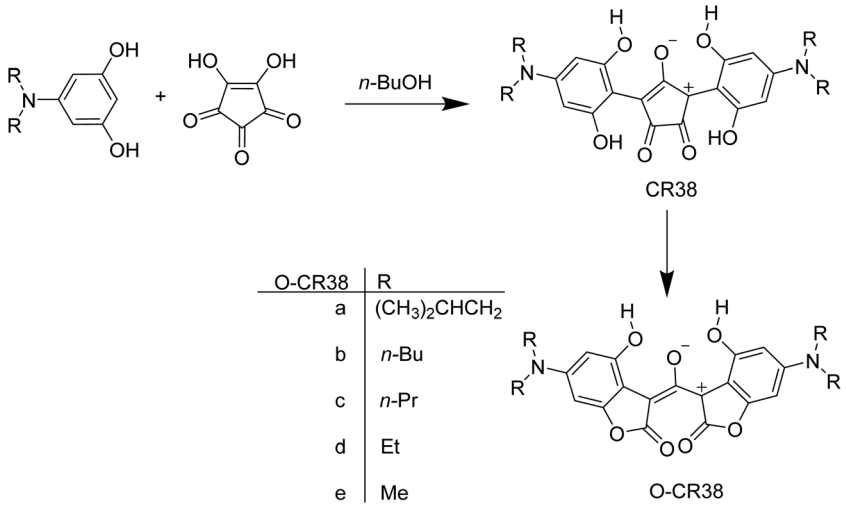

Scheme 13 O-CRs with absorption maxima at approximately 1100 nm.

and widely exploited in biomedical applications.[7–16,58,81,86] For example, Li *et al.*[86] synthesized a CR (CR21, Tables 1, 2 and Fig. 5) with absorption in the range of 650–850 nm, investigating it as a theranostic agent. Semicroconaines showed intense absorption spectra in protic solvents, with an extinction coefficient, ε, of about 10^3–10^4, lower than CRs, in general. With the decrease in organic solvent polarity (from MeOH to CH_2Cl_2), generally a hypsochromic shift was observed. For example, the absorption maximum of S-CR1 shifted from 574 nm in MeOH to 552 nm in CH_2Cl_2 (Scheme 8 and Fig. 5),[59] whereas the absorption profiles of nonsymmetric CRs were similar to those observed for symmetric indolenine-based CRs.[53] In Fig. 6, the representative absorption spectra of symmetric (CR5 and CR6, Scheme 6) and nonsymmetric (CR25a–c, Scheme 8) CRs are reported. Nonsymmetric CRs showed absorption maxima in the NIR region with high molar extinction coefficients in aprotic solvents (ε in the order of 10^5). As for semicroconaines, for nonsymmetric CRs, with the decrease in organic solvent polarity, a bathochromic shift was observed (*i.e.* the absorption maximum of CR25a shifted from 778 nm in MeOH to 802 nm in CH_2Cl_2; Fig. 5).[53]

Very recently, in 2024, Li *et al.*[87] proposed an interesting donor engineering approach to simultaneously manipulate the absorption and nonradiative transitions in CRs (Scheme 14). Increasing the electron donating ability of donor units, the absorption of CRs red-shift to the NIR-II region, especially when the benzo[*c*,*d*]indolinium donor group is used (CR39 Scheme 14). CR39 showed a narrower HOMO–LUMO energy gap and strong NIR-II light absorption ability. Moreover, the steric repulsion between the planar donor unit and the croconate acceptor in CR39 promotes the formation of a twisted intramolecular charge transfer state, promoting the decay of absorbed energy towards heat-producing and non-radiative pathways. The photothermal conversion efficiency of CR39 was found to be 84%.

Moreover, in 2024, Chen *et al.*[19] proposed the use of chalcogen atoms to modulate the absorption properties of CRs with the structure of CR2 (Scheme 4). By investigating four different chalcogen atoms (O, S, Se and Te), it was found that the absorption of CR can be shifted from the NIR-I to the NIR-II range due to the heavy-atom effect. The Te-substituted CR in its nanoformulation showed high NIR-II photothermal conversion

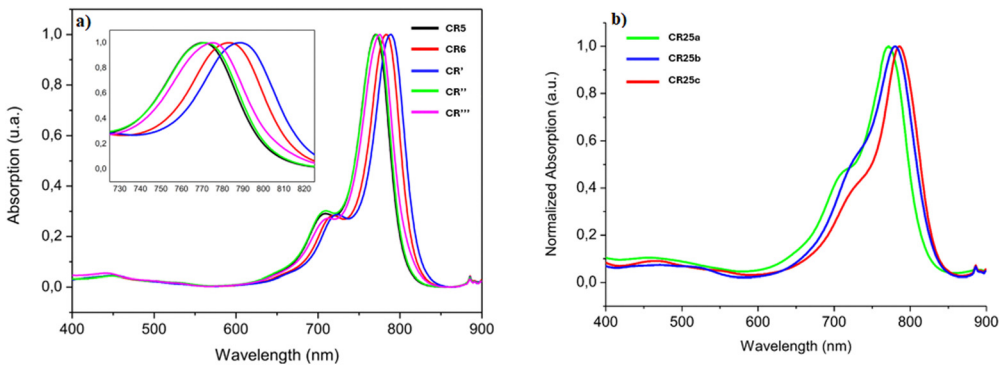

Fig. 6 Representative absorption spectra of CR5 and CR6 (a) and CR25a–c (b). Reproduced with permission from ref. 56 and 59. Copyright 2016, the Royal Society of Chemistry; copyright 2018, the American Chemical Society.

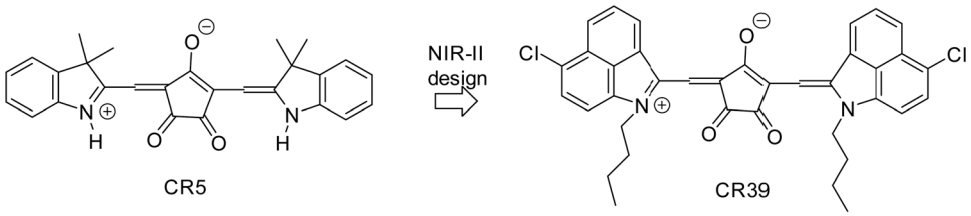

Scheme 14 Donor engineering of CR39.

efficiency (70.6%) and good photostability, resulting in superior potential in photothermal therapy for tumor elimination upon irradiation at 1064 nm.

4.1.2 Fluorescence. CRs show good photothermal conversion capabilities, as a result of intrinsic high non-radiative relaxation and thermal energy decay, so that they generally exhibit poor fluorescence, which limits applications in fluorescent technologies. In a US patent of 2002 by SurroMed,[88] for example, CRs were reported as bridged fluorescent dyes. However, the patent was focused on squaraine and cyanine families as fluorescent dyes and even if the structure of some CRs was reported together with that of squaraines and cyanines, no fluorescent data were provided for the CRs. In 2022, Pang *et al.*[15] exploited the fluorescence property of a water-soluble NIR-absorbing CR based on a thiophene-CR rigid core and two symmetric triethylene glycol chains for a NIR fluorescence imaging-guided synergistic photothermal/photodynamic therapy of cancer (CR40, Fig. 7 and Table 2).

CR40 exhibited a strong absorption peak at 780 nm with a high molar extinction coefficient of 1.19×10^5 M^{-1} cm^{-1} and a fluorescence peak at 815 nm exploited for *in vivo* fluorescence imaging. Li *et al.*[86] reported the data of fluorescence also for CR21 (Tables 1, 2 and Fig. 5), with a band in the range of 1000–1400 nm. The quantum yields (QYs) were recovered for both CR21 alone and CR21-PEG-GBP (CR21 conjugated with NH_2-PEG_{36}-COOH and targeting peptide GBP) assembled in DMSO and found to be 0.406% and 0.626%, respectively, related to carbon nanotubes (QY: 0.03%). The data of fluorescence were also reported by Capozzi *et al.*[59] for S-CRs, which showed a solvent polarity-dependent emission. In fact, for example, under the same measurement conditions and with the same concentration of about 10^{-6} M, S-CR1 (Scheme 8) showed the most intense emission in CH_2Cl_2, while S-CR2 showed the most intense emission in H_2O (Table 2). On the contrary, the non-symmetric CRs CR25a–c (Scheme 8) did not show any significant fluorescence in the range of 800–1000 nm.

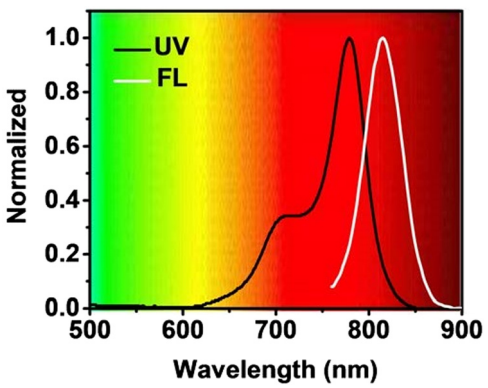

Fig. 7 Representative normalized absorption and fluorescence spectra of CR40. Reproduced with permission from ref. 15. Copyright 2022, the Royal Society of Chemistry.

4.1.3 Nonlinear optical properties. CRs exhibit nonlinear optical properties with the polarization strictly dependent on the intensity of the applied electromagnetic field. This dependence gives rise to various useful properties such as self-focusing, two-photon absorption, and third harmonic generation. The D–A–D molecular structure of CRs ensures high polarizability and extensive intramolecular charge transfer (ICT) in both the ground state and the lowest excited singlet state of molecules. The induced dipole moment (along a particular axis), which results from this charge transfer, can contribute to both the electronic and the reorientational mechanisms of the refractive index dependence on the electric field. Li *et al.*[54,55] investigated the third-order optical nonlinearities (NLO) of a CR involving the indolenine ring as the donor unit, both in the THF solution and into poly(methyl methacrylate) (PMMA) films. The NLO properties were measured by the femtosecond degenerate four-wave mixing (DFWM) technique under resonant conditions. The magnitude of the third-order nonlinear optical susceptibility in organic molecules and polymers spans in a broad range, depending on the resonance and non-resonance contributions, the former being several-fold larger than the latter. The DFWM response of the CR in PMMA films was found to be very fast and the contribution from the population grating was small (the effective third-order nonlinear susceptibility (χ_e) of the PMMA coating films was measured to be of the order of 10^{-8} esu). Three years earlier, Tian *et al.*[41] demonstrated that J-aggregates are suitable for NLO applications, fabricating thin films of O-CR38a (Scheme 13) on glass substrates by spin-coating from a 1 wt% $ClCH_2CH_2Cl$ solution. The spin-coated film of CR38a exhibited a broad absorption band peaked at 1228 nm. Compared to the absorption in the solution (about 1100 nm), the absorption of the spin-coated film is red-shifted by 135 nm, indicating the formation of J-like aggregates in the solid layer. Then, they investigated the third-order NLO susceptibility at 1.3 μm of the spin-coated films of CR38a using the Z-scan technique, demonstrating its high capability as a NLO material. Performing investigations based on experimental and theoretical techniques such as UV-visible spectra, DFWM, density functional theory, time-dependent density

functional theory, and symmetry-adopted cluster-configuration interaction (SAC-CI), in 2008, Prabhakar *et al.*[89] studied the non-resonant third-order NLO of CRs. Their results suggested that the large oxyallyl ring size and diradical character in CRs determine the third-order NLO properties and not the donor groups, as considered previously. These achievements were also supported by Maeda *et al.* in 2023,[45] who claimed that molecules with an intermediate open-shell character have an enhanced third-order NLO response and consequently two-photon absorption (TPA) activity, since the intermediate open-shell character can also be understood as a diminishment of covalency at the π-bonds, allowing the electron distribution along the π-conjugated system to distort more easily.

4.2 Electrochemical properties

CRs show semiconducting properties, with intense absorption bands in the visible and NIR region, thanks to a molecular biradical character which reduces the band gap. Theoretical calculations, as well as spectroscopic and voltammetry measurements, support these semiconducting properties. In 2008, Thomas *et al.*,[43] investigated a series of CRs (18 molecules) by DFT and SF-TDDFT study, reporting the HOMO and LUMO values estimated, together with the HOMO–LUMO gap (HLG). In the framework of CRs studied, for some structures surveyed in the present review, they found the values reported in Table 3:

In 2016, Punzi *et al.*[56] investigated, by absorption and CV measurements, a series of indolenine-based CRs, including CR5 and CR6 (Scheme 6). From oxidation and reduction potentials, they estimated the HOMO energy levels to be −5.25 and −5.33 and the LUMO energy levels to be −3.95 and −4.03 eV for CR5 and CR6, respectively (Fig. 8).

They also determined the optical (from absorption spectra) and electrochemical band gap E_g values: the E_g^{opt} values were 1.55 and 1.52 and the E_g^{elec} values were both 1.30 eV for CR5 and CR6, respectively. Theoretical calculations[43] were also performed on CR5, reporting an overestimation of the HOMO–LUMO band gap with respect to experimental results.[56] In 2023, Maeda *et al.*[45] investigated the electrochemical properties of CR2a and CR2b by cyclic voltammetry, determining the HOMO and LUMO energy levels and the resulting band gaps. They estimated for CR2a the HOMO and the LUMO levels to be −4.71 and −3.99 eV, respectively, for CR2b the HOMO and LUMO levels to be −4.66 and −3.91 eV, respectively (Fig. 9). As a result, the electrochemical band gap E_g^{elec} was found to be 0.72 for CR2a and 0.75 for CR2b.

Table 3 Symmetry, HOMO, LUMO and HLG for CRs from DFT and SD-TDDFT studies. Data were obtained from ref. 43

CR	Symmetry	HOMO[a] (eV)	LUMO[a] (eV)	HLG[a] (eV)
CR3a 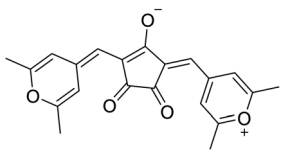	C_{2v}	−4.83	−3.35	1.48
	C_s	−4.86	−3.35	1.51
CR3b 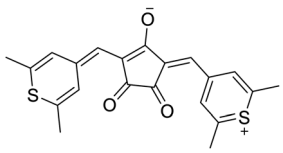	C_{2v}	−4.86	−3.56	1.30
	C_s	−4.89	−3.56	1.33
CR3c 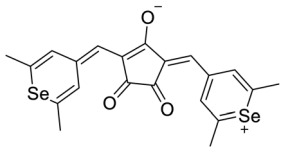	C_{2v}	−4.89	−3.65	1.25
	C_s	−4.92	−3.65	1.27
CR5 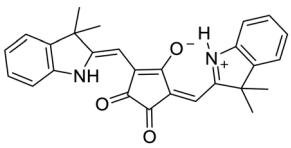	C_s	−5.05	−3.27	1.78
CR16 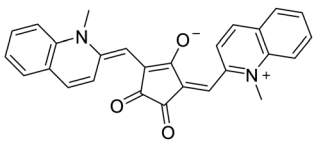	C_1	−4.73	−3.19	1.54

[a] Calculated at the RB3LYP/6-311+G(d,p) level.

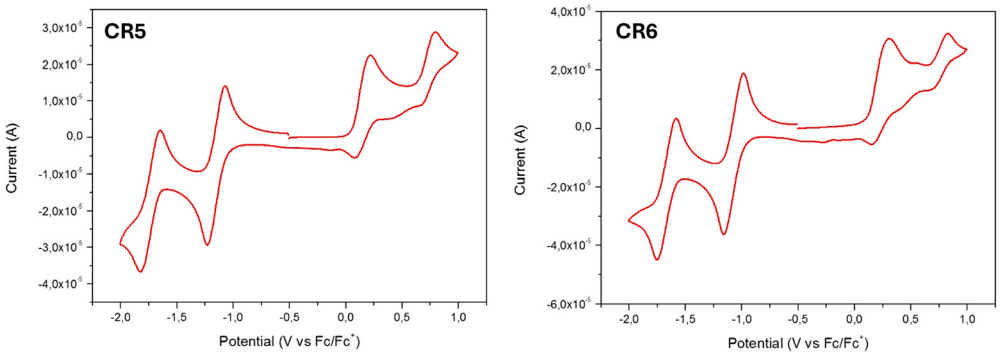

Fig. 8 Cyclic voltammograms of CR5 and CR6. Reproduced with permission from ref. 56. Copyright 2016, the Royal Society of Chemistry.

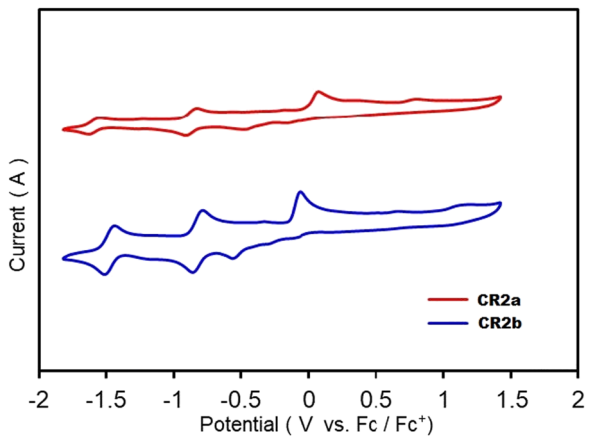

Fig. 9 Cyclic voltammograms of CR2a and CR2b. Reproduced with permission from ref. 45. Copyright 2023, the Royal Society of Chemistry.

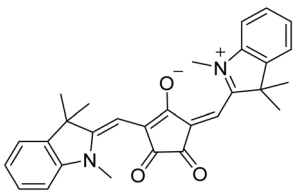

Scheme 15 Structure of CR41.

4.2.1 Charge carrier mobility. Croconic acid-based materials show three types of conductivity: semiconductivity, photoconductivity and proton conductivity. In 1993 Havinga *et al.*[75] exploited squaraine and croconaine-based polymers, polysquaraines and polycroconaines, to propose and explain the idea that conjugated polymers with alternate donor and acceptor moieties in the main chain are characterized by a small band gap. They reported new polymers with band gaps down to 0.5 eV, conductivities around 10^{-5} S cm^{-1} and stability in air up to 250 °C or higher. Punzi *et al.*[56] reported for the first time the charge carrier mobility of a series of indolenine-based CRs employed as an ambipolar active layer in organic thin-film transistors. They determined the value of the saturation hole ($\mu_{sat,p}$) and electron ($\mu_{sat,n}$) mobility of two CRs: CR5 $\mu_{sat,p} = (2.3 \pm 0.3) \times 10^{-5}$ cm^2 V^{-1} s^{-1} and $\mu_{sat,n} = (3.8 \pm 0.1) \times 10^{-6}$ cm^2 V^{-1} s^{-1}; CR6 $\mu_{sat,p} = (2.3 \pm 0.5) \times 10^{-5}$ cm^2 V^{-1} s^{-1} and $\mu_{sat,n} = (3 \pm 1) \times 10^{-6}$ cm^2 V^{-1} s^{-1} (Scheme 6). The electrical characterization of the two CRs revealed that both compounds exhibited an ambipolar behaviour, arising from the low band gap of the molecules (in the range of 1.27–1.32 eV), the charge separation within the croconic moiety and from the favourable energy level alignment at the metal–electrode interface. In 2008, Davidenko *et al.*[90] investigated the effect of different additives, including CR41 (Scheme 15), squarilyum, merocyanine and cationic polymethine dyes, on the photoconductive properties of films based on a co-oligomer of glycidylcarbazole with butylglycidyl ether. They concluded that the CRs possess greater capability of charge separation in the excited state, due to: (i) the HOMO level of CR41 with a higher energy than that of the HOMO level of the carbazole core, so this leads to an increase in the photoconductivity of the films as a result of the increase of the electron-transition probability from the carbazole core to the CR41, when it is in an excited state; (ii) in the excited state, CR41 is characterized by a pronounced bipolar structure of the indolenine donor groups, so the probability of intermolecular electron transition is strongly affected by the electrostatic interaction of these electrically charged donor groups and the carbazole core; and (iii) a large number of oxygen atoms in the structure of the CR41.

In 2019,[91] the same research group studied the photoelectric properties of films of polymeric composites (FPC) derived from poly-*N*-epoxypropylcarbazole (PEPC) and CR41. The composites were found to have hole-type photoconductivity. The internal photoelectric effect is therefore a function of the photogeneration of charge carriers from the CR dye and transport of the holes along the donor fragments of the polymer matrix. Very interesting in CRs is, also, proton conduction, which was investigated for the first time only very recently in 2022 by Taylor *et al.*[67] They prepared a porous organic polymer *via* polycondensation between a tripodic indole-based monomer and croconic acid (POP, P-CR30a, Scheme 11). The CR-based polymer with a zwitterionic structure was found to be a relatively weak proton conductor (1.9×10^{-7} S cm^{-1} at 90 °C and 90% relative humidity). However, doping this polymer with LiCl vastly improves the proton conductivity up to a value of 0.15 S cm^{-1} at 90 °C and 90% relative humidity. In 2023, Enoch *et al.*[76]

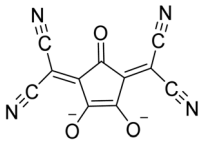

CR42

Scheme 16 Structure of CR42.

performed measurements of conductivity on compressed cylindrical pellets of polymer P-CR30b (Scheme 11), finding very low values (in the order of 10^{-7} S m^{-1}) for the pristine materials, which results in substantial insulation. Following doping with iodine, P-CR30b showed a substantial increase in conductivity, with values up to 0.1 S m^{-1}.

4.2.2 Multiple oxidation states in croconic acid-based compounds. In a recent work, Armstrong *et al.*[92] proposed a croconate violet derivative ($Croc^{2-}$, CR42, Scheme 16) as a new promising anionic redox organic material for applications in non-aqueous redox flow batteries (RFB). The voltammetry measurements disclosed the high number of oxidation states accessible by $Croc^{2-}$, highlighting a high intrinsic capacity for low-molecular-weight redox active organic molecules.

This molecule is very interesting from an electrochemical point of view thanks to its high proportion of redox-active functional groups for molecular unit. Furthermore, it is air-stable and easy to handle. This is a rare example of CR obtained by reacting croconic acid with an electron-acceptor unit, the malononitrile. We have included in the present review this croconic acid derivative for its great potential in energy applications (see the following section for energy storage applications).

5. Applications

5.1 Data recording and data storing

The capability of CRs to convert light energy adsorbed by means of various photophysical and photochemical processes into other forms of energy, strictly connected to their chemical structure, can be exploited in data recording and storage media.[31] Effectively, the optical data recording capability of CRs was the first property reported in the first patent published on the argument.[61] This patent reported the preparation of new CRs (Scheme 6) and their suitability as agents for sensitizing photographic elements and photoconductive compounds. CRs were easily incorporated into the organic thin films acting as recording layers. This property was appealing in CRs also for their high stability to heat and light, so that most of patents from 1970 to 1999 covered the use of CRs in optical recording media,[48,64,93–96] where a semiconductor laser was used for writing a record and the CR as a laser-responsive layer with improved light stability and durability. However, no patents published since 2000 covered this application.

5.2 Photothermal applications

A singular application of NIR-absorbing CRs was proposed in a 2001 patent,[84] where they, together with other infrared absorbing compounds such as phthalocyanines, 2,3-napthalocyanines and squaraines, were used to improve the reheat rate of a container preform. The container preform was composed of a polymer suitable to produce a stretch blow molded bottle and, at least, one organic NIR-absorbing material able to absorb at least twice as much light in the range 700–1200 nm as in the range 400–700 nm. The NIR-absorbing component being present in sufficient amount to improve the reheat rate of the container preform. This property known as photothermal heating capability was explored some years later by Smith's research group that can be considered the pioneer of the studies of laser-induced photothermal heating capability of CRs.[57] In this work, three important findings achieved with the CR26/rotaxane system (Scheme 9) are reported: (a) NIR-absorbing CRs exhibit properties such as high-performance photothermal heating, intense and narrow absorption band at around 800 nm, high chemical, photo- and thermal stability, very efficient relaxation to the ground state and very low oxygen photosensitization ability; (b) photothermal heating obeys the Beer–Lambert law ($1 - 10^{-A}$) and sample heating reaches an asymptotic limit when the chromophore absorbance values are greater than $\sim$1; and (c) CRs form red-shifted encapsulation complexes which allows the realization of molecular recognition induced activated photothermal heating. Pang *et al.*[15] reported a photothermal conversion efficiency (PCE) of 77% for CR40 (Table 2) upon 735 nm laser irradiation, while Tang *et al.*[6,97] reported PCEs of 72.7% and 79.5% for CR24 (Scheme 17 and Table 1) and CR43 (Scheme 17), respectively, upon 808 nm laser irradiation. In their work,[6] Tang *et al.* exploited the light harvesting ability and high photothermal conversion efficiency of CR43, to fabricate a self-healing flexible film with poly(dimethylsiloxane). The small molecule CR43 was investigated for highly efficient utilization of solar energy, showing excellent photothermal performance in the aggregated state.

After aggregation, CR43 exists in a dimeric form, stabilized by strong π–π intermolecular interactions, and displays a rarely reported high-spin state. Benefiting from the synergistic effects of radical features and strong π–π intermolecular interactions, it absorbs broadly from 300 to 2000 nm. In-depth investigations

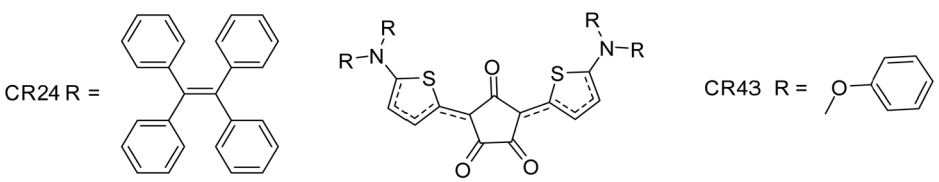

Scheme 17 Structures of CR24 and CR43.

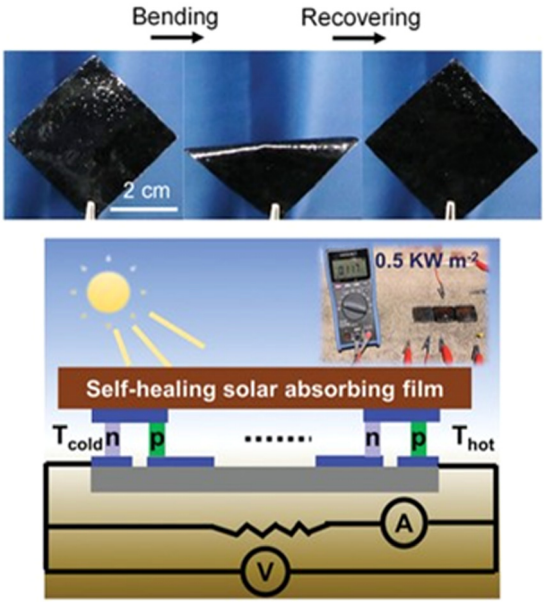

Fig. 10 Illustration of the excellent flexibility of the H-PDMS/CR43 film (top) and schematic illustration of the STEG device (bottom). Reproduced with permission from ref. 6. Copyright 2022, Wiley.

with transient absorption analyses reveal that strong intermolecular π–π interactions can promote nonradiative relaxation by accelerating internal conversion and facilitating intermolecular charge transfer (ICT) between dimeric molecules to open internal conversion pathways. Finally, exploring the applications of CR43 for solar-thermal applications, a flexible self-healing poly(dimethylsiloxane) (H-PDMS)/CR43 film was created as a solar absorber for an organic–inorganic composite flexible solar thermoelectric generation (STEG) system, which achieved an open circuit output voltage of 192 mV and a maximum power density of 1.86 W m^{-2} at a solar irradiance of 5 kW m^{-2} (Fig. 10).

NIR-absorbing photothermal CRs also find application as mesogenic calamitous materials. Yang *et al.*[71] explained how, thanks to the photothermal heating effect induced by the CR (YHD796 in Fig. 11, labelled as CR36b in this review, Fig. 5), well dispersed in a LCE (liquid crystalline elastomer) matrix, the composite film obtained performs a completely reversible contraction/expansion response towards the NIR light stimulus.

They reported the first example of a NIR-absorbing mesogenic organic magnet. Moreover, the same research group, utilized the same CR36b (YHD796) to prepare a new biomimetic composite material capable of performing two different three-dimensional reversible transformations (bending *versus* chiral twisting) through modulation of the wavelength of the light stimuli, miming one individual plant tendril material (Fig. 11).[98] In 2017, Liu *et al.*[99] exploited the NIR absorbing YHD796C chromophore (Fig. 12) as a soft actuator material able to increase the local temperature from 18 to 260 °C in 8 s and lift up weights 5600 times heavier than its own weight,

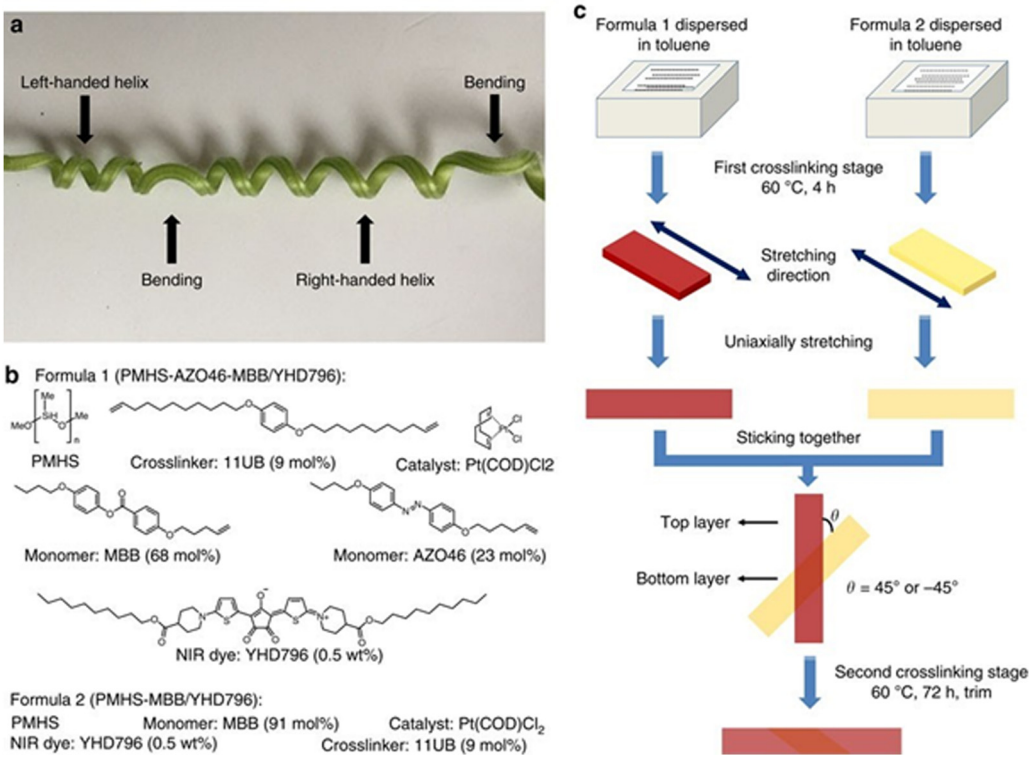

Fig. 11 New biomimetic composite material. (a) The image of a cucumber plant tendril with bending and chiral twisting distorsion. (b) The chemical compositions of PMHS-AZO46-MBB/YHD796 composite (Formula 1) and PMHS-MBB/YHD796 composite (Formula 2). (c) Schematic illustration of the preparation protocol of the dual-layer LCE ribbon material. Reproduced with permission from ref. 98. Copyright 2016, Springer Nature.

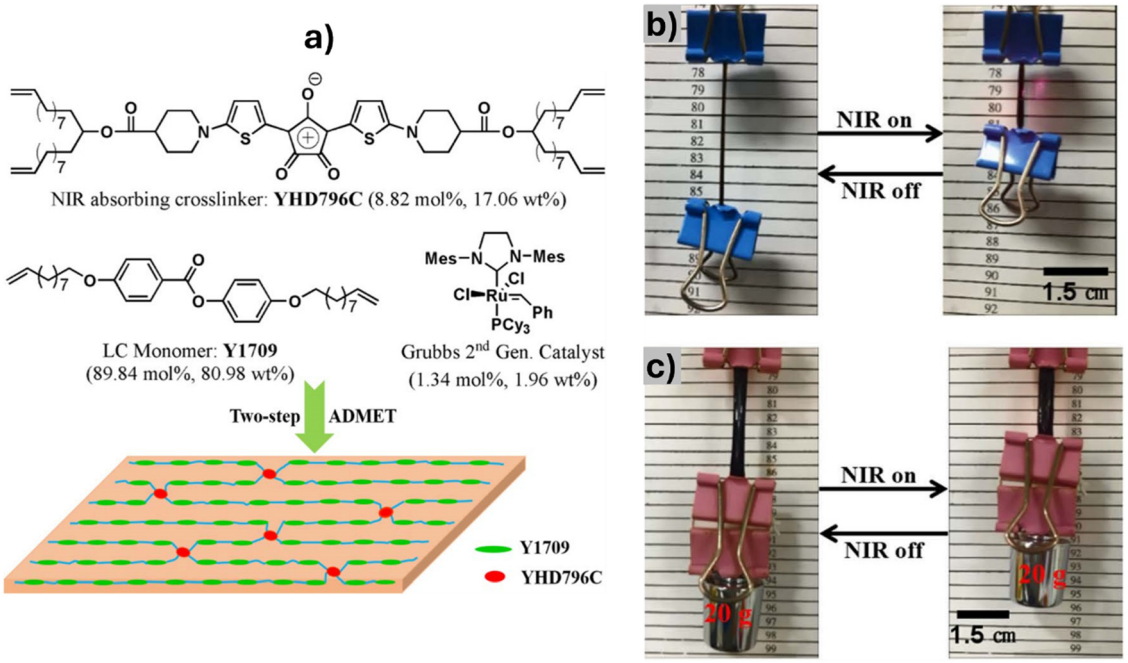

Fig. 12 (a) Chemical composition of the LCE material; (b) photo image of an LCE ribbon before and after NIR (808 nm) irradiation; and (c) photo image of an LCE film (4.3 mg) lifting up a load (*ca.* 24.44 g) under NIR irradiation. Reproduced with permission from ref. 99. Copyright 2017, the American Chemical Society.

under 800 nm NIR irradiation. The NIR absorbing chromophore YHD796C was designed with cross-linkable functional groups (four alkenyl-tailed groups) and submitted to *in situ* acyclic diene metathesis polymerization with a LC monomer (Y1709, Fig. 12) to fabricate a uniaxial aligned main-chain LCE soft actuator material, in which the NIR chromophore is chemically bonded in the LCE material. The resulting soft actuator material exhibited an ultrafast photoresponsive speed and superior mechanical property, easily lifting up heavy loads, even up to 5680 times heavier than their own weight.

Following this, Nie *et al.*[100] prepared a photothermally responsive liquid crystal elastomer using the same CR36b (YHD796) as the photothermal agent in order to produce single-faced Möbius strip actuators capable of producing continuous *in situ* rotation under NIR irradiation (Fig. 13).

A 2014 patent[101] reports the use of CRs as additives to plastics to facilitate laser welding of these materials. Dyes usually used as laser absorbers must meet certain requirements: (a) intense absorption at the wavelength of the laser used; (b) heat resistance during the welding process; and (c) neither the dye nor the decomposition products shall be toxic when used together with foodstuffs and the like. CRs used in welding applications are shown in Scheme 18. These CRs are easy to adapt to plastic materials. In fact, by changing the substituents on the amino nitrogen, it is possible to modulate the solubility, while, through an appropriate selection of the aromatic or heteroaromatic group, it is possible to set the absorption profile of the dye.

In 2019,[102] another patent disclosed a new NIR-absorbing CR suitable for use in NIR laser welding methods of plastic materials. In the same year, another patent describes the use of CRs as photothermal dyes to be mixed with thermoplastic PEEK polymers for the purpose of creating articles by 3D printing.[103] Very recently, in 2024, Xu *et al.*[104] reported the use of a CR with the basic structure of CR32 to functionalize the surface of polypropylene with a CR-functionalized polymer acting as an antifouling and NIR-light-mediated photothermal sterilizing agent. The CR was designed with a reactive functional group (alkyl bromide) suitable for polymerization and used to prepare various amphiphilic block polymers acting as antibacterial coatings of polypropylene substrates.

5.3 Biomedical applications

In the biomedical field, fluorescent CRs can be exploited as phototherapeutic agents for applications in synergistic photothermal/photodynamic therapy of cancer guided by NIR fluorescence imaging.[15] In this application, a water-soluble NIR CR labelled as TCR (CR40 in this review, Table 2) was used, characterized by intense NIR absorption, high molar extinction coefficient of 1.19×10^5 M^{-1} cm^{-1} and fluorescence that picked at 780 and 815 nm, respectively. TCR showed a high photothermal conversion efficiency (77%) and capability of generating hydroxyl radicals under 735 nm laser irradiation. All these properties allowed us to exploit the TCR in successfully performing fluorescence imaging-guided synergistic photothermal/photodynamic cancer therapy. The photothermal properties have suggested the possibility of using CRs as organic agents for photoacoustic (PA) or optoacoustic (OP) imaging, an emerging technique in the field of high-performance molecular imaging, which is very useful in the

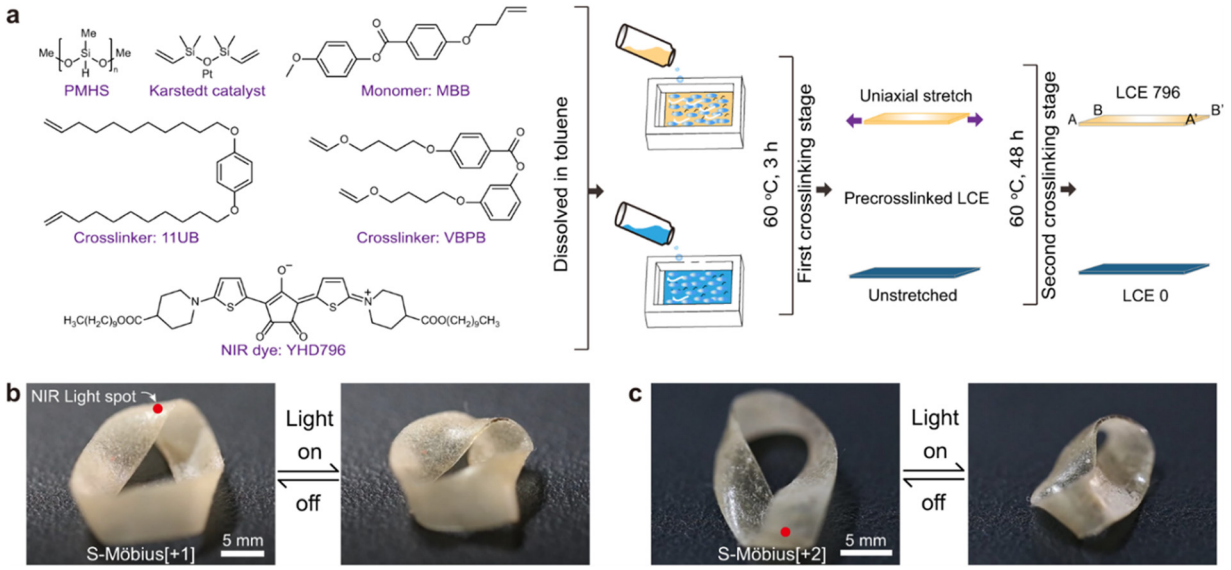

Fig. 13 Dual-layer polysiloxane-based liquid crystal soft actuators. (a) Schematic illustration of the chemical components of this LCE system and the preparation procedure of LCE796 (orange part) and LCE0 (dark blue part) ribbons. Photographs of the single-layered (b) S-Möbius[+1] and (c) S-Möbius[+2] actuators upon application of a photothermal stimulus (scale bars: 5 mm) Reproduced with permission from ref. 100. Copyright 2021, Springer Nature.

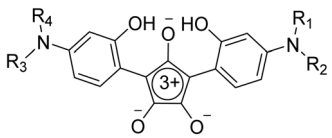

Scheme 18 CR33-type dyes used in welding applications.

biomedical field. In general, optimal photophysical characteristics of PA (OP) agents include: (i) intense absorption, (ii) low fluorescence quantum yield, (iii) a well-defined spectral signature, and (iv) high photostability. Photoacoustic (optoacoustic) imaging (PAI or OAI) is a powerful non-invasive bioimaging technique achieved by mixing the contrast obtained from optical absorption with the generation of high-resolution images that reach deep tissue. PAI (OAI) can illuminate tissues at multiple wavelengths, and thus, provides anatomical images, offers images of the distribution of light-absorbing molecules by performing spectral unmixing. In this cotext, CRs thanks to their features appear to be the most promising materials for photoacoustic applications. PA applications of CRs have been published since 2016.[32,58,105,106] First, in 2016, Guha *et al.*[58] prepared some liposomes containing a pH-sensitive and NIR (808 nm)-absorbing CR rotaxane complex (CR44-rotaxane, Scheme 19(A)) and used it as an effective nanoparticle probe for the photoacoustic imaging of acidic pH at deep locations both *in vitro* and *in vivo*.

Liu Y. *et al.*[105] demonstrated that NIR CR probes can produce a strong photoacoustic signal when compared with other probes, at the same mass concentration. The NIR CRs used (one of them shown in Scheme 19(B), CR45) were designed and synthesized to specifically bind the cerebrovascular amyloid (binding energy −9.3 kcal mol^{-1}). They showed an intense absorption peak at 800 nm and generated a significant increase in local temperature under low-power laser irradiation. Liu H. *et al.*[107] expanded the application of PA imaging to the long-wavelength NIR-II region using an open-ring CR (O-CR38a, Scheme 13 and Fig. 5) with NIR-II absorption at 1094 nm (which may be the smallest molecule among the few small organic molecules with an absorption wavelength >1.0 μm). Jansen *et al.*,[108] for the first time, produced CR copolymer nanoparticles by reacting croconic acid with a range of aromatic diamines (P-CR46a–d, Scheme 19(C)). All synthesized polymers show broad absorption in the NIR region and therefore represent suitable candidates as contrast agents for PAI. It is possible to observe the highest photoacoustic activity for all polymers in the range of 820–920 nm. Currently, there is extensive research on therapies applied to cancer treatment, and some of them are being investigated at a clinical level. Some examples include tissue, cell and gene or RNA interference (RNAi) therapies, and other treatments use light to eliminate solid tumors, including photothermal therapies (PTTs). Regarding the latter, the basis of photothermal therapy consists of an agent (usually a nanoparticle or a dye) capable of absorbing light at a specific wavelength and releasing vibrational energy producing a local increase in heat. When this heat increases above 43 °C, protein denaturation is induced and thus tumor cell apoptosis occurs. CRs are promising candidates for PTT. They have a dual behavior depending on the environmental pH, changing their structure and absorption profile from an alkaline form (absorption peak in the visible region under slightly alkaline conditions, *i.e.* pH 7.4) to an acidic form (high absorption peak in the NIR region). Furthermore, CRs

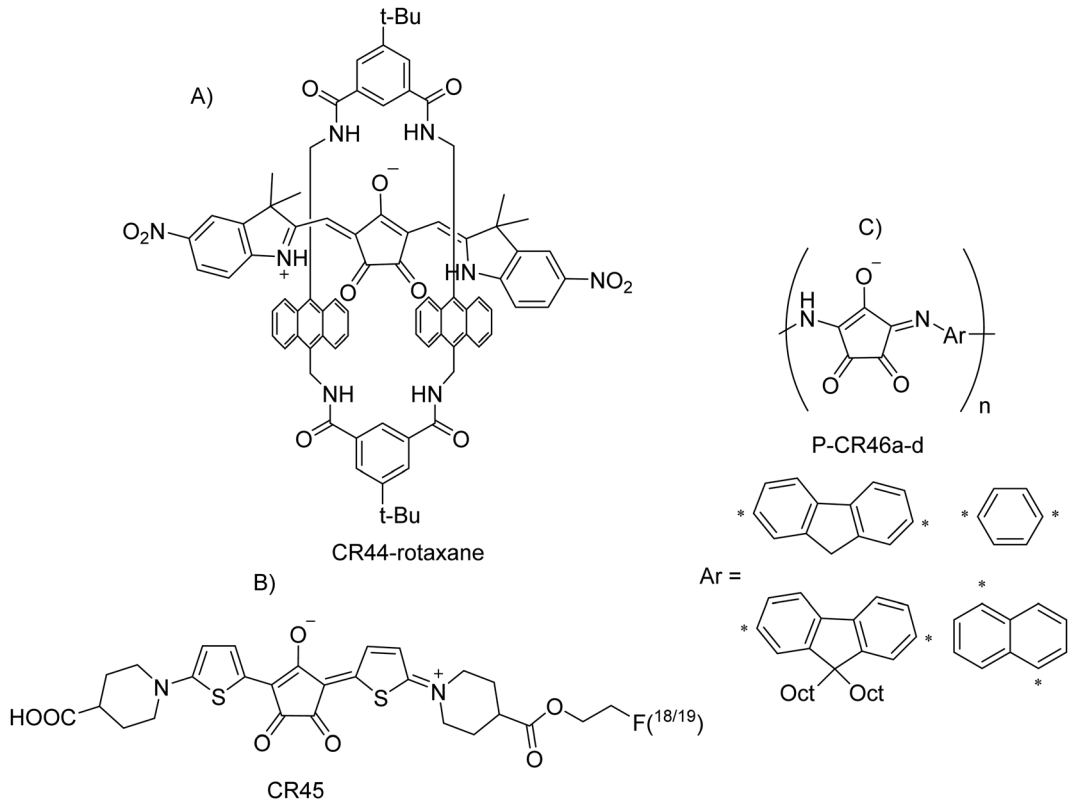

Scheme 19 (A) pH-Sensitive and NIR-absorbing CR44-rotaxane dye contained in liposomes. (B) NIR-CR dye, CR45. (C) Croconaine copolymer produced by reacting croconic acid with aromatic diamines, P-CR46a–d.

have strong resistance to photobleaching, chemical and thermal stability, and exhibit a short-excited state lifetime that underlies efficient relaxation. They also have very little fluorescence emission and reduced singlet oxygen generation; therefore, they constitute ideal dyes to decouple photodynamic effects from photothermal effects.[9] Interesting examples of PTT are nanoscale heat generation applications. Smith *et al.*[7] have demonstrated that CR rotaxanes can be used for clean photothermal heating of nanoparticles without producing singlet oxygen, explaining then the procedure for performing a photothermal heating experiment in a more recent work.[109] More recently, Liu *et al.*[16] demonstrated the high photothermal conversion efficiency of CR24-NPs (Table 1) (PCE ∼ 58%) and their ability to eliminate tumor *in vivo* using a low-energy laser, while remaining biocompatible and well tolerated. In 2021, Shahrivarkevishahi *et al.*[110] used CR21 (Table 2) to make a new generation of immune-photothermal agents using chemically modified virus-like particles (VLPs) called bacteriophage Qβ. This can generate more heat at 808 nm than free dye CR21 with a photothermal efficiency comparable to gold nanostructures, but it is biodegradable and acts as an immunoadjuvant united with the heat. Finally, Zhang *et al.*[111] designed and synthesized a functionalized cationic polymer (CR-PQAC) using CR21 as a bridging agent and quaternary ammonium groups for photothermally enhanced antimicrobial therapy under near-infrared irradiation (Fig. 14).

In 2024, Niu *et al.*[112] reported the use of CR44 to realize a thiol-triggered CR-chromene system to induce ferroptosis and photothermal synergistic efficient tumour ablation. Moreover, in 2024, Dong *et al.*[113] reported the use of CR24 to realize croconaine-based nanoparticles with absorption in the NIR-I region and fluorescence emission in the NIR-II region and their ability to induce significant tumor ablation without apparent side effects. Furthermore, they are able to promote the formation of antitumor immune memory in a colorectal cancer model. Finally, even in 2024, You *et al.*[114] investigated a CR containing two indole groups linked to two morpholine units as a lysosome-targeting and Fe^{3+}-modulate agent. The CR together with fibronectin-targeting peptides CREKA, Fe^{3+} and DSPE-PEG_{2000} were mixed for engineering nanoparticles for enhanced triple-mode bioimaging and Fe^{3+}-triggered tumour synergistic therapy. For a broader overview of investigation on CRs for bioimaging and phototherapy applications refer to the reviews of Cai *et al.*[11] and Kataria *et al.*[34]

5.4 Photovoltaic applications

The ability to transform collected light into other forms of energy can also be exploited in photovoltaic applications, where the light absorbed is converted into electricity. CR dyes, as light harvesting materials with high extinction coefficients, were investigated in dye-sensitized solar cell (DSSC) devices with the aim of improving the efficiency of solar cells. They can perform two key functions: (i) reduce internal energy loss resulting from energy mismatch for electron injection and dye regeneration and (ii) extend light collection in the NIR.

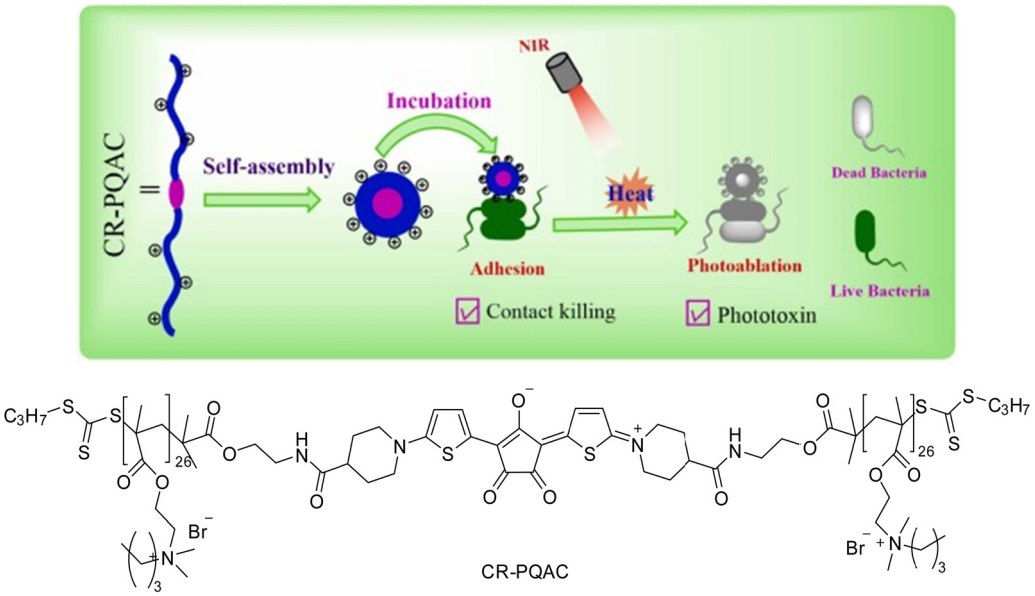

Fig. 14 Molecular structure of CR-PQAC and its antibacterial mechanisms. Reproduced with permission from ref. 111 (modified). Copyright 2024, Elsevier.

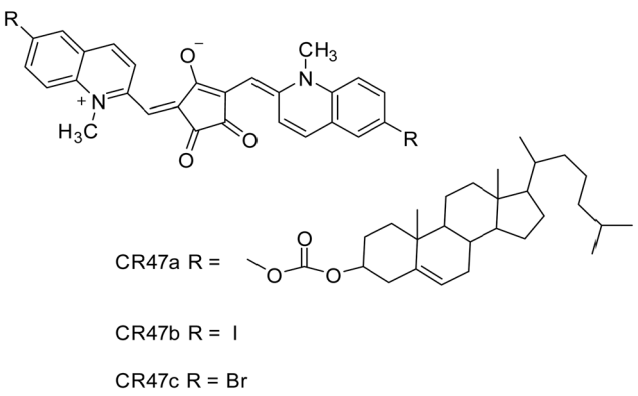

Scheme 20 CR47a–c investigated for harvesting infrared photons in DSSC devices.

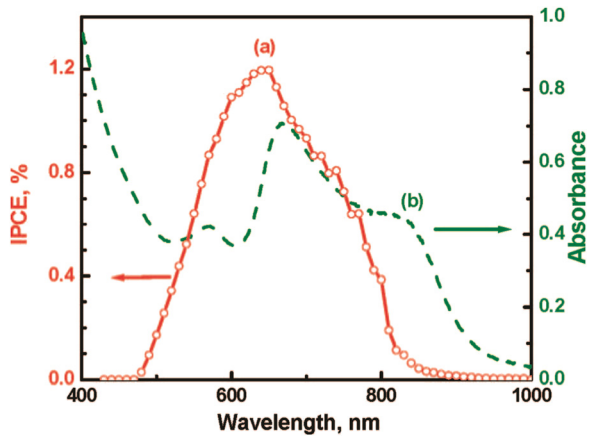

Fig. 15 Photocurrent response of the OTE/TiO_2/CR47a electrode to monochromatic illumination. The comparison of (a) IPCE and (b) absorbance traces shows the primary species responsible for photocurrent generation. Electrolyte: 0.5 M LiI and 0.05 M I_2 in CH_3CN. Reproduced with permission from ref. 2. Copyright 2008, the American Chemical Society.

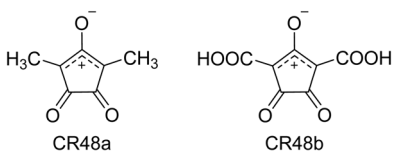

Scheme 21 CR48a and CR48b.

In 2008, Takechi *et al.*[2] reported the investigation of the light-harvesting ability of three CR dyes in photoelectrochemical cells. They studied the excited-state properties of CRs (CR47a,b,c, Scheme 20), with the aim of using them to harvest infrared photons. When deposited in thin films on optically transparent electrodes or nanostructured TiO_2 films, the CRs form H aggregates which are photoactive and produce anodic current. However, poor IPCE were obtained (IPCE of 1.2% at 650 nm for CR47a, the best performing) as a result of poor charge separation (Fig. 15).

In 2015, Chitumalla *et al.*[3] performed theoretical studies on the effect of the electron withdrawing/donating nature of substituents connected to the croconate ring on the geometric, electronic and optical properties of two CRs. They demonstrated the efficiency of CRs in dye-sensitized solar cells (DSSCs) starting from two structurally simple symmetric CRs (CR48a,b, Scheme 21). The high binding energy of diketone groups of CR dyes on the TiO_2 surface and the light-harvesting efficiency make CRs suitable for DSSC applications. Periodic density functional theory (DFT) calculations showed that the binding energy is strongly dependent on the nature of the

substituent present on the dyes, so that, by proper molecular and structural design, high-performance CRs can be achieved.

5.5 Sensing applications

Thanks to suitable optical properties, such as high photostability and high molar absorption, CRs could be exploited in sensing applications. Among the first researchers in this direction, we find the investigation on the acidochromic property of CRs.[21] Puyol *et al.*[22] synthesized and characterized six new CRs for use as long-wavelength chromioionophores in optochemical sensors. These indicators exploiting an acid–base balance involving the proton bonded to the indole nitrogen, showed intense absorptions in the far-visible, or NIR region, matching the power of some inexpensive, mass-produced diode lasers. Furthermore, the pK_a values cover a range from 2.8 to 12.6, with the possibility to modify the absorption band and the pK_a by acting on the structure and substituents of CRs. This leads to the possibility of combining CRs with commercially available ionophores for the development of ion-selective optodes, through the use of membranes that combine the selective recognition of an ionophore with the optical transduction of a chromoionophore, enclosed within a plasticized PVC membrane. Subsequently, a wider number of papers have been devoted to the use of CRs as metal ion sensors, by exploiting their chemical structure very suitable to bind metal ions. An interesting work from 2008 demonstrated, for the first time, the metal ion binding properties of CRs based on quinaldine as the donor group.[23] These CRs (CR47a, CR47b and CR47c, Scheme 20) showed low affinity for monovalent ions and high affinity for divalent metal ions, mainly Zn^{2+}, Pb^{2+} and Cd^{2+}, forming complexes with 2 : 1 stoichiometry and high association constants of the order of 10^{11}–10^{14} M^{-2} (Fig. 16).

The binding between CRs and divalent metal ions occurred on the carbonyl groups of the croconate ring, as demonstrated by ^{1}H NMR spectra, leading to relevant chelation-enhanced fluorescence. In 2015, a highly selective and sensitive chemosensor, (2,5-bis[(4-carboxyl-piperidylamino)thiophenyl]-croconaine), BCTC (labeled as CR21 in this review, Table 1), was synthesized and investigated for the detection of Fe^{3+} and Cu^{2+}.[24] The metal ions coordinate with the oxygen anion of CR21 with 1 : 1 stoichiometry of the host–guest complexation. Furthermore, a key aspect is the high specificity of this chemosensor for Fe^{3+} and Cu^{2+} also in the presence of other metal ions, with the colorimetric and fluorescence changes observed, something, also by the naked eye. Since 2017, other articles reported CRs with the capacity of sensing a specific metal ion, *i.e.* Fe^{3+}, Hg^{2+}, Ag^{+}, and Cu^{2+}. In particular, the research group of Yao synthesized and investigated two different CRs both with high specificity for Fe^{3+},[25,26] 2,5-bis[2,3,3-trimethyl-3*H*-indole-5-sulfonic acid]-croconaine (TISC) and 2,5-bis[3-benzyl-2-methylbenzothiazole]-croconaine (BMC) (Fig. 17).

The TISC results a highly selective water-soluble optical probe for Fe^{3+}, with a binding constant of 3.071 × 10^4 M^{-1} and 1 : 1 stoichiometry of complexation *via* N atoms and O of oxalyl unit. BMC results in a highly selective optical probe for Fe^{3+} with a binding constant of 1.4244 × 10^4 M^{-1} and 1 : 1 stoichiometry of complexation *via* the carbonyl groups of

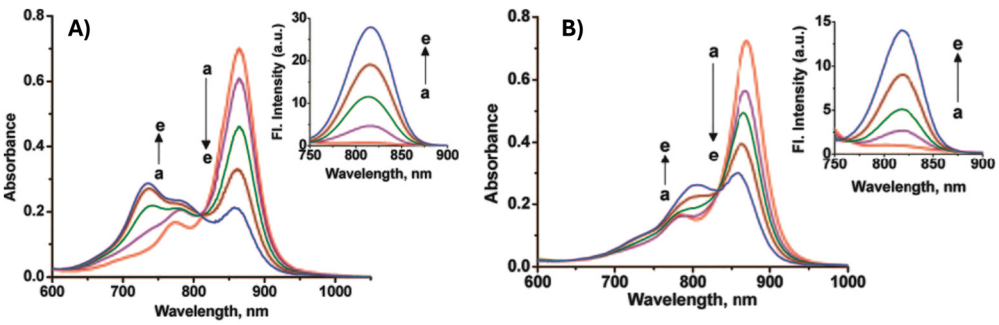

Fig. 16 Changes in the absorption spectra of CR47a (7.75 μM) in THF with addition of (A) Pb^{2+} [Pb^{2+}] = 0 (a), 0.94 (b), 1.88 (c), 2–82 (d) and 3.87 μM (e) and (B) Cd^{2+} [Cd^{2+}] = 0 (a), 0.94 (b), 1.88 (c), 2–82 (d) and 3.87 μM (e). The insets show the corresponding changes in fluorescence intensity. Excitation wavelength = 700 nm. Reproduced with permission from ref. 23. Copyright 2008, the American Chemical Society.

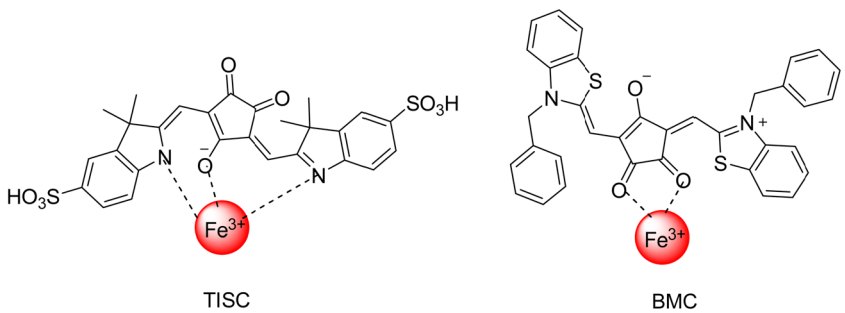

Fig. 17 CRs: TISC and BMC binding Fe^{3+}.

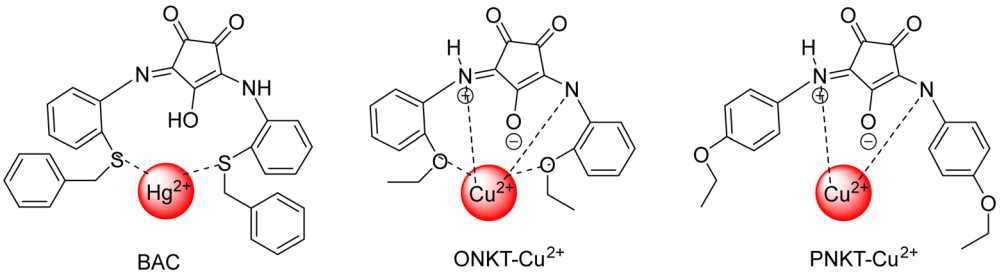

Fig. 18 CRs: BAC binding Hg^{2+} and ONKT and PNKT binding Cu^{2+}.

croconate ring. Moreover, BAC results in a highly selective optical probe for Hg^{2+}, with a binding constant of 1.6×10^5 M^{-1} and 1 : 1 stoichiometry of complexation *via* S atoms (Fig. 18).[27] The high selectivity of all three of these CRs even in the presence of many other interferent metal ions, together with their NIR-absorbing property, makes them potential sensors for biomedical applications in the detection of metal ions in human organisms.

The detection of heavy and transition metal ions, such as Pb^{2+}, Cd^{2+}, Hg^{2+}, Cu^{2+}, and Fe^{3+}, has been attracting increasing attention for environmental safety and human health. For example, an excess or decrease in Fe^{3+} can impair cellular homeostasis and cause various disorders such as anemia, Alzheimer's disease, diabetes, Parkinson's disease, cancer, Huntington's disease, and heart failure. In addition, trace amounts of mercury accumulated in the body cannot be excreted through the body's metabolism, leading to heart, liver and thyroid diseases and causing nervous disorders, chronic mercury poisoning, and even tumors. Therefore, the detection of Fe^{3+} and Hg^{2+} is significant for the diagnosis and treatment of diseases. In 2021, Wang *et al.*[115] investigated CR1 (Scheme 7) as a highly sensitive and selective colorimetric and fluorescent probe for the detection of Ag^{+}. They performed measurements also in the presence of potentially competitive ions (Na^{+}, K^{+}, Mg^{2+}, Ca^{2+}, Co^{2+}, Ni^{2+}, Zn^{2+}, Cd^{2+}, Ba^{2+}, Al^{3+}, and Cr^{3+}) and found a high selectivity of CR1 for Ag^{+}, without interference from other metals. In 2022, He *et al.*[116] reported two new CRs, ONKT and PNKT (Fig. 18), similar to BAC, in which the 2-ethoxyaniline and 4-ethoxyaniline were used as donor groups to bind croconic acid, instead of 2-benzylthioaniline of BAC. These CRs resulted in highly selective and sensitive colorimetric probes for Cu^{2+}. Very recently, very interesting investigations have been devoted to polymeric derivatives of CRs for application in gas sensing. Yu *et al.*,[77] using the polycroconaine P-CR31a (Scheme 12), demonstrated the possibility to exploit the ion-in-conjugation concept to realize organic gas sensors operating at 100 °C and 70% relative humidity. The P-CR31a-based sensor resulted in having a ppb detection limit for NO_2, showing the highest sensitivity (2526 ppm^{-1} at 40 ppb) between all reported NO_2 chemiresistive sensors. Moreover, by exploiting the ion-in-conjugation concept, Zhou *et al.*[78] fabricated a hybrid system with Mxene $Ti_3C_2T_x$ and polycroconaine P-CR31b (Scheme 12) suitable for NH_3 detection. P-CR31b was obtained by *in situ* polymerization in the presence of $Ti_3C_2T_x$ to yield a core–shell composite $Ti_3C_2T_x$@P-CR31b exhibiting good sensitivity (2.8% ppm^{-1}), selectivity, repeatability and fast response/recovery for NH_3 detection. The presence of P-CR31b significantly improved the long-term stability of the $Ti_3C_2T_x$@P-CR31b with respect to pristine $Ti_3C_2T_x$. In the same year, 2023, Chen *et al.*,[79] still relying on the ion-in-conjugation, fabricated a humidity sensor based on the polycroconaines P-CR31c and P-CR31d for snoring monitoring. The sensor was able to monitor human breath with rapid response/recovery, working in a wide range of relative humidity (11–95% RH) and with a time stability of 8 h. Finally, this year Wang *et al.*[80] reported the results of the investigation on the ion-in-conjugation polymer P-CR31e for gas sensing under humid conditions. The P-CR31e-based gas sensor exhibited an ultrahigh sensitivity of 802.7 ppm^{-1} at 1 ppm, sub-ppb detection limit and high selectivity under humid air (80% humidity) at temperatures down to 350 K.

5.6 Energy storage

Recently, Armstrong *et al.*[92] have suggested the applications of croconic acid-based compounds in the field of energy storage, by investigating the dianion croconate violet CR42 as a symmetric redox active organic molecule (ROM) for promising non-aqueous redox flow battery electrolytes (RFBs) (Scheme 22 and Fig. 19).

CR42 was applied in an acetonitrile electrolyte and used as both the battery posolyte and negolyte, with a cell potential of 1.82 V and a concentration of 1 M. Experiments conducted using CR42 as the posolyte and 2,1,3-benzothiadiazole or tetracyanoquinodimethane as the negolyte showed improved battery performance, indicating the potential of croconic derivatives in battery technology. This molecule is the only example reported in the literature where a croconic acid dye has been investigated for battery applications, as well as croconic acid salts,[117–120] which have been widely studied and are considered very promising in this field.

6. Challenges and perspectives

In summary, the structural and synthetic aspects, chemico-physical properties and applications of croconic acid-based materials were thoroughly reviewed. They are very easy to synthesize by low-cost

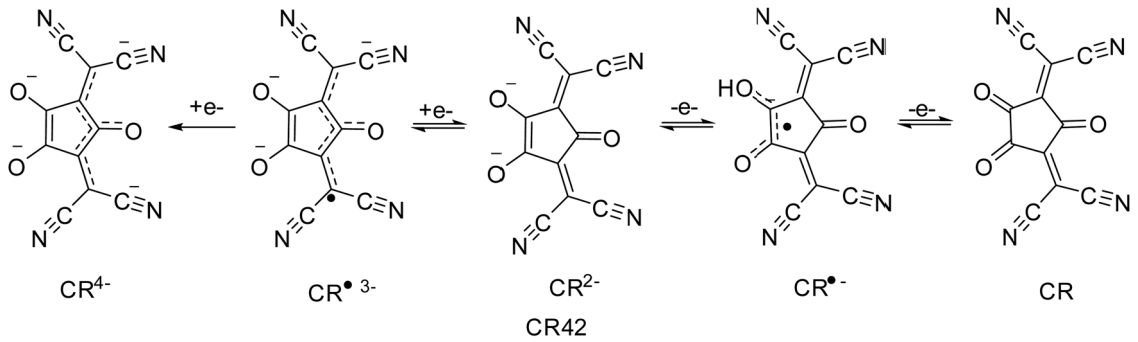

Scheme 22 CR42 redox series.

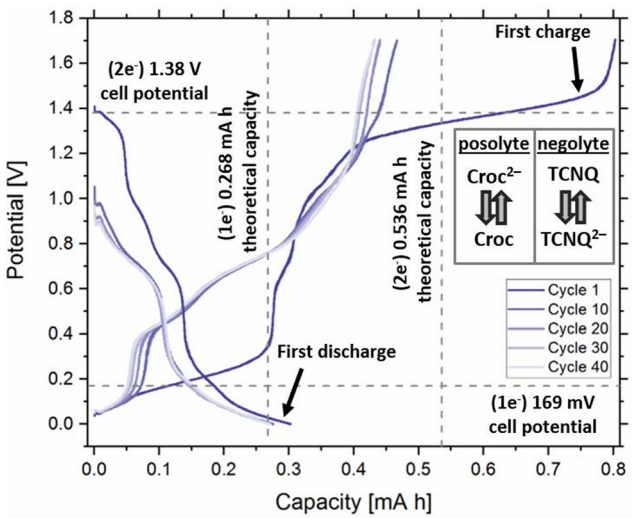

Fig. 19 Asymmetric battery charge–discharge curves of 1 mM TBA_2CR42 *vs.* 1 mM TCNQ mixed electrolytes in 0.1 M $TBAPF_6$, MeCN electrolyte at 0.48 mA cm^{-2}. The upper and lower threshold potentials are 1.7 and 0 V, respectively. Celgard porous separator. Reproduced with permission from ref. 92. Copyright 2019, Elsevier.

methodologies and under mild conditions, showing intense NIR absorption with high molar extinction coefficients, thermal stability, high photobleaching resistance and intrinsic biocompatibility as well as structural, electrical and optical tunability, which make them organic functional materials with high potential in many applications. The molecular structure of this class of organic compounds is very versatile and can be designed with functional groups which allow further reactivity aimed at conjugating other units and functionality able to tailor the chemico-physical properties and applications. In recent years, croconic acid-based materials have been developing rapidly and considerable progress has been achieved in the applications. Photothermal properties, intrinsic biocompatibility and NIR-absorbing capacity have driven the research mainly in investigating their potential application in the emerging field of theranostics. Most of the publications, in fact, focus on their use in biomedical field, as theranostic agents for the treatment of tumours, by the photothermal therapy (PTT). However, several challenges are still open for future biomedical applications and clinical implementation: (a) usually, except for O-CR36a, they show very short singlet excited-state lifetime with highly efficient relaxation to the ground state and negligible ISC to the triplet state, which make them suitable for PAI instead of fluorescence imaging (FLI). However, PAI present a lower sensitivity than that of FLI and then lower performance in biological imaging, and hence, the design of new CR structures guided by theoretical calculation should be addressed to overcome this issue; (b) since until today CRs have been tested only at the animal level (mice), to meet clinical requirements more systematic and complex investigations are necessary, such as biokinetics, biodegradation, potential long-term toxicity, biodistribution, pharmacokinetics, immune reactions in large animals, interactions and possible risks with biological systems. CR-based nanoformulation has been detected as a valid strategy to improve the optical performance and stability aimed at overcoming critical issues such as biocompatibility, bioavailability, tumour-targeting and multifunction. The NIR-absorbing property and the ability to complex metal ions (strictly related to the croconate unit) have driven the research also in investigating the potential of CRs as sensors of metal ions, especially heavy metal ions strongly impacting on both the environment and human health. Despite the excellent, versatile and easily modulated ligand capabilities of CRs, very limited studies have been conducted on their sensing properties. Only a few articles reported data on the selective sensing of metal ions such as Fe^{3+}, Hg^{2+}, Pb^{2+}, Cd^{2+} and Zn^{2+}, lacking a systematic and deep investigation on other metal ions, and overall, on tailored CR structures for specific metal ions. The wide structure tunability allows modifying the molecular skeleton by additional functional groups, with the right spatial position with respect to the croconate unit, arranging a final ligand system able to coordinate with high specificity any metal ion. In this direction, the research potential appears very wide, starting from the design and synthesis of new CRs to the study and application in metal ion detection. Conversely, the first studies on CRs, in particular patents, were focused on their application in optical data storage. Almost all patents were related to the application of CRs as the active matrix of organic thin film recording layer, by exploiting irradiation by laser light. CRs ensure excellent properties such as high stability to heat and light, high sensitivity and durability for reading for many times. Notwithstanding,

also in this field, the investigation appears lacking, and a deeper study should be addressed to highlight all potential of this class of organic compounds. For example, the NIR-absorbing capability of CR dyes could be exploited in product code labelling, marking products and using an IR laser for reading, for an effective fight against counterfeiting and the protection of brands. At the same time, the NIR-absorbing properties of CRs can be exploited also in the development of IR protection and camouflage materials, a research area with a broad military implication, and part of the more general stealth technology aimed at rendering objects unidentifiable. However, to date, the electrical properties of croconic acid-based materials have received poor consideration and only very few papers investigated them. Generally, these materials, both molecules and polymers, belong to materials with a low band gap, a class of materials which would show high intrinsic conductivity (without doping) and better transparency in the visible region. Only one paper reports the investigation of a very simple croconate derivative, the croconate violet, as a very promising anionic redox active organic posolyte in redox flow batteries. Despite the preliminary interesting results, this study has not been followed by further investigations aimed at revealing all the potential of croconic acid-based materials in the field. Based on the limits of undesirable radical disproportionation phenomena accounting for poor capacity retention, brought to light by the only work carried out, further investigations deserve to be conducted, starting from chemico-structural variations, aimed at enhancing radical stability and then capacity retention in the device. In light of the priorities that current society pursues in the energy sector, research in the field of batteries plays a key role and croconic acid-based materials could offer properties and then technological solutions in line with the set goals, therefore, worthy of extensive and careful investigation. Furthermore, the numerous papers devoted to the investigations of croconic acid salts for battery applications should support the interest to study croconic acid-based organic dyes, the subject of the present review, in this direction. The scientific demand of developing research on the electrical properties of croconic acid-based materials is also supported by the results obtained with microporous polymers based on CRs, which when appropriately doped with LiCl show super-proton conduction. This evidence, combined with the capacity of intense and broad absorption in the visible spectrum up to the NIR region, should stimulate interest of studies for organic photovoltaic applications. On the contrary, very few investigations have been carried out and even limited to applications in DSSC cells, reporting very low IPCE values as a result of poor charge separation. Studies, both theoretical and experimental, aimed to investigate the bulk heterojunction (BHJ) and perovskite solar cell applications are completely missing. Properties such as high extinction coefficient, tuneable charge carrier mobility, and absorption in the NIR region should prompt the researchers to investigate the potential of CRs in photovoltaic applications as both active matrixes and additive materials. In perspective, while the optical properties have been extensively investigated and the application potential well defined together with the open challenges, the electrical properties await broader and more in-depth investigations, starting from the synthetic aspects, to access new structures with improved charge transport capacities, to move on structure–properties correlation studies aimed to clarify their potential in strategic technological sectors such as batteries, photovoltaics, and electrochemical cells for hydrogen production and storage. Furthermore, the biradical character of this class of materials implies magnetic properties, making them very attractive in key technologies such as magnet-based motors and generators for large power generation, energy storage, transmission, and spintronics. Furthermore, extensive and relevant investigations on the optical and electrical properties in the solid state are also lacking, especially in the light of application in solid layer-based devices. In this direction, the chemical synthesis can play a key role in controlling the solid-state aggregation and then the chemico-physical properties in solid, driving future research towards specific applications. We hope that the present review attracts the interest of academic and industrial researchers towards this very intriguing class of organic functional materials, especially in the less explored fields.

Data availability

No primary research results, software or code have been included, and no new data were generated or analysed as part of this review.

Conflicts of interest

There are no conflicts to declare.

Acknowledgements

This work was financially supported by MUR, project PON ARS01_00951_V0584, D.D. n. 2051 del 02/08/2018, titled ''ECOTEC – Smart and eco-sustainable fibres and tissues for technical clothing and high fashion'' and project PON 2014–2020 – MIUR – ARS01_00869 CUP: B95F21001900005, titled ''PERCIVAL – Processi di EstRazione di bioprodotti da sCarti agroIndustriali e VALorizzazione in cascata''.

References

1 D. E. Lynch and D. G. Hamilton, *Eur. J. Org. Chem.*, 2017, 3897–3911.
2 K. Takechi, P. V. Kamat, R. R. Avirah, K. Jyothish and D. Ramaiah, *Chem. Mater.*, 2008, **20**, 265–272.
3 R. K. Chitumalla, M. Lim, X. Gao and J. Jang, *J. Mol. Model.*, 2015, **21**, 297.
4 T. S. Ranwaha, N. E. Maluta and R. R. Maphanga, *Proc. SAI*, 2018, 247–252.
5 T. Ranwaha, I. Elegbeleye, N. Maluta and R. Maphanga, *Mater. Express*, 2020, **10**, 1917–1924.
6 J. Sun, E. Zhao, J. Liang, H. Li, S. Zhao, G. Wang, X. Gu and B. Z. Tang, *Adv. Mater.*, 2022, **34**, 2108048.

7 S. Guha, K. Shaw, G. T. Spence, F. M. Roland and B. D. Smith, *Langmuir*, 2015, **31**, 7826–7834.
8 Q. Chen, X. Liu, J. Zeng, Z. Cheng and Z. Liu, *Biomaterials*, 2016, **98**, 23–30.
9 T. Alejo, C. Font, M. Abad, V. Andreu, V. Sebastian, G. Mendoza and M. Arruebo, *J. Photochem. Photobiol., A*, 2019, **382**, 111936.
10 S. Lei, Y. Zhang, N. T. Blum, P. Huang and J. Lin, *Bioconjugate Chem.*, 2020, **31**, 2072–2084.
11 Y. Cai, Y. Pan, L. Liu, T. Zhang, C. Liang, X. Mou, X. Ye, W. Wang and X. Dong, *Coord. Chem. Rev.*, 2023, **474**, 214865.
12 S. Lv, Y. Miao, D. Liu and F. Song, *ChemBioChem*, 2020, **21**, 2098–2110.
13 N. Liu, P. O'Connor, V. Gujrati, D. Gorpas, S. Glasl, A. Blutke, A. Walch, K. Kleigrewe, M. Sattler, O. Plettenburg and V. Ntziachristos, *Adv. Healthcare Mater.*, 2021, **10**, 2002115.
14 X. Xu, Y. He and Y. Wang, *Cell Rep. Phys. Sci.*, 2021, **2**, 100433.
15 E. Pang, R. Huang, S. Zhao, K. Yang, B. Li, Q. Tan, S. Tan, M. Lan and B. Wang, *J. Mater. Chem. B*, 2022, **10**, 9848–9854.
16 N. Liu, P. O'Connor, V. Gujrati, P. Anzenhofer, U. Klemm, K. Kleigrewe, M. Sattler, O. Plettenburg and V. Ntziachristos, *Nanophotonics*, 2022, **11**, 4637–4647.
17 P.-D. You, C.-R. Ouyang, F. Lu, C. Zeng, H.-D. Cai, G.-S. Shi, L. Liu and C.-Q. Zhou, *J. Photochem. Photobiol., B*, 2023, **245**, 112748.
18 C.-R. Ouyang, P.-D. You, F. Lu, H. Mei, J.-L. Yu, Z. Zhu and C.-Q. Zhou, *Dye Pigm.*, 2024, **221**, 111780.
19 X. Chen, X. Ma, G. Yang, G. Huang, H. Dai, J. Yu and N. Liu, *ACS Appl. Mater. Interfaces*, 2024, **16**, 12332–12338.
20 J. Li, X. Su and N. Liu, *Sens. Actuators, B*, 2024, **408**, 135535.
21 C. Encinas, E. Otazo, L. Rivera, S. Miltsov and J. Alonso, *Tetrahedron Lett.*, 2002, **43**, 8391–8393.
22 M. Puyol, C. Encinas, L. Rivera, S. Miltsov and J. Alonso, *Dyes Pigm.*, 2007, **73**, 383–389.
23 R. R. Avirah, K. Jyothish and D. Ramaiah, *J. Org. Chem.*, 2008, **73**, 274–279.
24 S. Wang, T. Cong, Q. Liang, Z. Li and S. Xu, *Tetrahedron.*, 2015, **71**, 5478–5483.
25 S. Ye, C. Zhang, J. Mei, Z. Li, S. Xu, X. Li and C. Yao, *J. Photochem. Photobiol., A*, 2017, **347**, 130–137.
26 S. Ye, Q. Liang, Z. Li, S. Xu and C. Yao, *Tetrahedron*, 2017, **73**, 1350–1357.
27 Z. Xu, C. Zhang, X. Zheng, Z. Li and S. Xu, *Optik*, 2018, **175**, 54–62.
28 T. Ranwaha, I. Elegbeleye, N. Maluta and R. Maphanga, *Mater. Express*, 2020, **10**, 1917–1924.
29 X.-F. Cheng, C. Yu, J.-X. Liu, Z.-S. Zhang, J. Wang, W. Ye, Q. Cao, J.-H. He and J.-M. Lu, *Sens. Actuators, B*, 2021, **345**, 130317.
30 J. Fabian and R. Zahradník, *Angew. Chem., Int. Ed. Engl.*, 1989, **28**, 677–694.
31 M. Emmelius, G. Pawlowski and H. W. Vollmann, *Angew. Chem., Int. Ed. Engl.*, 1989, **28**, 1445–1471.
32 R. E. Borg and J. Rochford, *Photochem. Photobiol.*, 2018, **94**, 1175–1209.
33 H. S. Jung, P. Verwilst, A. Sharma, J. Shin, J. L. Sessler and J. S. Kim, *Chem. Soc. Rev.*, 2018, **47**, 2280–2297.
34 S. Kataria and D. Sareen, *J. Anal. Chem.*, 2024, **79**, 15–28.
35 *Oxocarbons*, ed. R. West, Elsevier, 2012, pp. 59–77.
36 P. V. R. Schleyer, K. Najafian, B. Kiran and H. Jiao, *J. Org. Chem.*, 2000, **65**, 426–431.
37 C. Prabhakar, K. Yesudas, G. Krishna Chaitanya, S. Sitha, K. Bhanuprakash and V. J. Rao, *J. Phys. Chem. A*, 2005, **109**, 8604–8616.
38 K. Srinivas, C. Prabhakar, C. Lavanya Devi, K. Yesudas, K. Bhanuprakash and V. Jayathirtha Rao, *J. Phys. Chem. A*, 2007, **111**, 3378–3386.
39 A. Tripathi, Promila and C. Prabhakar, *J. Phys. Org. Chem.*, 2017, **30**, e3673.
40 H. Langhals, *Angew. Chem., Int. Ed.*, 2003, **42**, 4286–4288.
41 M. Tian, S. Tatsuura, M. Furuki, Y. Sato, I. Iwasa and L. S. Pu, *J. Am. Chem. Soc.*, 2003, **125**, 348–349.
42 A. L. Puyad, C. Prabhakar, K. Yesudas, K. Bhanuprakash and V. J. Rao, *J. Mol. Struct.*, 2009, **904**, 1–6.
43 A. Thomas, K. Srinivas, C. Prabhakar, K. Bhanuprakash and V. J. Rao, *Chem. Phys. Lett.*, 2008, **454**, 36–41.
44 D. López-Carballeira, D. Casanova and F. Ruipérez, *ChemPhysChem*, 2018, **19**, 2224–2233.
45 T. Maeda, T. Oka, D. Sakamaki, H. Fujiwara, N. Suzuki, S. Yagi, T. Konishi and K. Kamada, *Chem. Sci.*, 2023, **14**, 1978–1985.
46 T. P. Simard, J. H. Yu, J. M. Zebrowski-Young, N. F. Haley and M. R. Detty, *J. Org. Chem.*, 2000, **65**, 2236–2238.
47 A. Treibs and L. Schulze, Pyrrol-Farbstoffe der Krokonsäure und Rhodizonsäure, *Liebigs Ann. Chem.*, 1973, **1973**, 201–206.
48 K. Katagiri, Y. Oguchi and Y. Takasu, US4548886, 1985; K. Katagiri, Y. Oguchi, T. Ohtake, K. Arao and Y. Takasu, US4629670, 1986; K. Katagiri, Y. Oguchi, T. Ohtake, K. Arao, M. Kitahara and Y. Takasu, US4673630, 1987.
49 Y. Oguchi, K. Katagiri and Y. Takasu, US4738908, 1988.
50 Y. Oguchi and T. Santoh, *Optical recording medium*, US4921780, 1990.
51 Y. Inagaki, T. Hioki, N. Makino, K. Adachi and Y. Suzuki, US4851322, 1989.
52 N. Zappimbulso, M. A. M. Capozzi, A. Porcheddu, G. M. Farinola and A. Punzi, *ChemSusChem*, 2021, **14**, 1363–1369.
53 G. T. Spence, S. S. Lo, C. Ke, H. Destecroix, A. P. Davis, G. V. Hartland and B. D. Smith, *Chem. – Eur. J.*, 2014, **20**, 12628–12635.
54 Z. Li, Z. H. Jin, K. Kasatani and H. Okamoto, *Phys. B*, 2006, **382**, 229–234.
55 Z. Li, S. Xu, L. Niu, Z. Zhang and Z. Chen, *SPIE Procee. Nonlinear Opt.: Techn. Appl.*, 2008, **6839**, 683910.
56 A. Punzi, M. A. M. Capozzi, V. Fino, C. Carlucci, M. Suriano, E. Mesto, E. Schingaro, E. Orgiu, S. Bonacchi, T. Leydecker, P. Samori, R. Musio and G. M. Farinola, *J. Mater. Chem. C*, 2016, **4**, 3138–3142.
57 G. T. Spence, V. H. Gregory and B. D. Smith, *Chem. Sci.*, 2013, **4**, 4240–4244.

58 S. Guha, G. K. Shaw, T. M. Mitcham, R. R. Bouchard and B. D. Smith, *Chem. Commun.*, 2016, **52**, 120–123.
59 M. A. M. Capozzi, A. Punzi, F. Babudri, R. Musio and G. M. Farinola, *J. Org. Chem.*, 2018, **83**, 14396–14405.
60 W. Liu, E. M. Peck and B. D. Smith, *J. Phys. Chem. B*, 2016, **120**, 995–1001.
61 G. A. Rillaers and H. Depoorter, DE1930224, 1970.
62 G. A. Rillaers and H. Depoorter, US3615417, 1971.
63 G. A. Rillaers and H. Depoorter, US3793313, 1974.
64 S. Yasui, M. Matsuoka and T. Kitao, *Dyes Pigm.*, 1989, **10**, 13–22.
65 V. E. de Oliveira, R. Diniz, F. C. Machado and L. F. C. de Oliveira, in: *Cross Conjugation: Modern Dendralene, Radialene and Fulvene Chemistry*, ed. H. Hopf and M. S. Sherburn, 2016, pp. 117–144.
66 F. Colmenero and R. Escribano, *J. Phys. Chem. A*, 2019, **123**, 4241–4261.
67 D. Taylor, X. Hu, C. Wu, J. M. Tobin, Z. Oriou, J. He, Z. Xu and F. Vilela, *Nanoscale Adv.*, 2022, **4**, 2922–2928.
68 K. Katagiri, Y. Oguchi and Y. Takasu, US5079128, 1992.
69 D. Keil, H. Hartmann and C. Reichardt, *Liebigs Ann. Chem.*, 1993, 935–939.
70 X. Song and J. W. Foley, *Dyes Pigm.*, 2008, **78**, 60–64.
71 L. X. Guo, M. H. Liu, S. M. Sayed, B. P. Lin, P. Keller, X. Q. Zhang, Y. Sun and H. Yang, *Chem. Sci.*, 2016, **7**, 4400–4406.
72 E. E. Havinga, W. ten Hoeve and H. Wynberg, *Polm. Bull.*, 1992, **29**, 119–126.
73 E. E. Havinga, A. Pomp, W. ten Hoeve and H. Wynberg, *Synth. Met.*, 1995, **69**, 581–582.
74 D. M. De Leeuw, E. E. Havinga, A. H. Alberts, G. J. Meekes and A. J. W. Tol, EP0603939B1, 1994.
75 E. E. Havinga, W. Ten Hoeve and H. Wynberg, *Synth. Met.*, 1993, **55**, 299–306.
76 S. Enoch, A. B. Nipate, V. Lakshimi and R. R. Malakalapalli, *Chem. Commun.*, 2023, **59**, 8846–8849.
77 C. Yu, J.-H. He, X.-F. Cheng, H.-Z. Lin, H. Yu and J.-M. Lu, *Angew. Chem., Int. Ed.*, 2021, **60**, 15328–15334.
78 J. Zhou, S. H. H. Shokouh, L. Cui, T. Jarvinen, O. Pitkanen, Z.-P. Lv and K. Kordas, *Nanoscale Horiz.*, 2023, **8**, 794–802.
79 Z.-K. Chen, W.-W. Bai, Y.-Q. Huo and J.-H. He, *Sens. Diagn.*, 2023, **2**, 721–725.
80 J. Wang, J.-L. Wei, Q. Cao, X.-F. Cheng, Z.-K. Chen and J.-H. He, *ACS Sens.*, 2024, **9**, 236–243.
81 L. Tang, F. Zhang, F. Yu, W. Sun, M. Song, X. Chen, X. Zhang and X. Sun, *Biomaterials*, 2017, **129**, 28–36.
82 N. Liu, V. Gujrati, J. Malekzadeh-Najafabadi, J. P. F. Werner, U. Klemm, L. Tang, Z. Chen, J. Prakash, Y. Huang, A. Stiel, G. Mettenleiter, M. Aichler, A. Blutke, A. Walch, K. Kleigrewe, D. Razansky, M. Sattler and V. Ntziachhristos, *Photoacoustics*, 2021, **22**, 100263.
83 S. J. Telfer, R. P. Short, S. G. Stroud, A. J. Puttick, S. M. Ramos and M. J. Zuraw, WO1992009661, 1992.
84 B. E. Maxwell, M. A. Weaver, J. J. Krutak, W. W. Parham, G. F. Rhodes and J. C. Fleischer, US6197851, 2001.
85 I. V. Kurdiukova, A. V. Kulinich and A. A. Ishchenko, *New J. Chem.*, 2012, **36**, 1564–1567.
86 S. Li, Y. Zhang, X. Liu, Y. Tian, Y. Cheng, L. Tang and H. Lin, *Theranostics*, 2022, **12**, 76–86.
87 J. Li, X. Su and N. Liu, *Sens. Actuators, B*, 2024, **408**, 135535.
88 R. Singh, G. Gorski and G. Frenzel, US6403807, 2002.
89 C. Prabhakar, K. Yesudas, K. Bhanuprakash, V. J. Rao, R. S. Santosh Kumar and D. N. Rao, *J. Phys. Chem. C*, 2008, **112**, 13272–13280.
90 N. A. Davidenko, Yu. P. Get'manchuk, E. V. Mokrinskaya, L. N. Gumenyuk, V. A. Pavlov, N. G. Chuprina, N. N. Kuranda, S. V. Khutornyī, A. A. Ishchenko, N. A. Derevenko, A. V. Kulinich, V. V. Kurdyukov and L. I. Kostenko, *J. Opt Technol.*, 2008, **75**, 182–186.
91 N. A. Davidenko, I. I. Davidenko, A. A. Ishchenko, I. V. Kurdiukova, E. V. Mokrinskaya, L. S. Tonkopieva and N. G. Chuprina, *Theor. Exp. Chem.*, 2019, **55**, 103–109.
92 C. G. Armstrong, R. W. Hogue and K. E. Toghill, *J. Power Sources*, 2019, **440**, 227037.
93 T. Sato, M. Umehara, M. Abe, H. Oba and Y. Ueda, US4656121, 1987.
94 T. Santoh, C. Mihara and H. Sugata, US5190849, 1993.
95 K. Katagiri, Y. Oguchi and Y. Takasu, US5278026, 1994.
96 K. Katagiri, Y. Oguchi and Y. Takasu, US5382497, 1995.
97 G. Chen, J. Sun, Q. Peng, Q. Sun, G. Wang, Y. Cai, X. Gu, Z. Shuai and B. Z. Tang, *Adv. Mater.*, 2020, **32**, 1908537.
98 M. Wang, B. P. Lin and H. Yang, *Nat. Commun.*, 2016, **7**, 13981.
99 L. Liu, M.-H. Liu, L.-L. Deng, B.-P. Lin and H. Yang, *J. Am. Chem. Soc.*, 2017, **139**, 11333–11336.
100 Z. Z. Nie, B. Zuo, M. Wang, S. Huang, X. M. Chen, Z. Y. Liu and H. Yang, *Nat. Commun.*, 2021, **12**, 2334.
101 T. Brock-Nannestad, M. Pittelkow and H. Ø. Bak, WO2014/166506A1, 2014.
102 A. Jeppesen, B. E. Nielsen, T. Brock-Nannestad and M. Pittelkow, WO154974, 2019.
103 C. U. Lee, A. J. Boydston, M. A. Ganter and D. W. Storti, US0275735A1, 2019.
104 X. Xu, H. Zhao, S. Ren, W. He, L. Zhang and Z. Cheng, *ACS Appl. Mater. Interfaces*, 2024, **16**, 46947–46963.
105 Y. Liu, Y. Yang, M. Sun, M. Cui, Y. Fu, Y. Lin, Z. Li and L. Nie, *Chem. Sci.*, 2017, **8**, 2710–2716.
106 N. Liu, K. Mishra, A. C. Stiel, V. Gujrati and V. Ntziachristos, *Adv. Drug Delivery Rev.*, 2022, **189**, 114506.
107 H. Liu, X. Wang, Y. Huang, H. Li, H. Peng, H. Yang, J. Li, H. Hong, Z. Lei, X. Zhang and Z. Li, *ACS Appl. Mater. Interfaces*, 2019, **11**, 30511–30517.
108 F. Jansen, M. Lamla, D. Mauthe, S. Fischer, H. Barth and A. J. C. Kuehne, *Macromol. Rapid Commun.*, 2020, **41**, 2000418.
109 H. H. McGarraugh, W. Liu, B. P. Matthews and B. D. Smith, *Eur. J. Org. Chem.*, 2019, 3489–3494.
110 A. Shahrivarkevishahi, M. A. Luzuriaga, F. C. Herbert, A. C. Tumac, O. R. Brohlin, Y. H. Wijesundara, A. V. Adlooru, C. Benjamin, H. Lee, P. Parsamian, J. Gadhvi, N. J. De Nisco and J. J. Gassensmith, *J. Am. Chem. Soc.*, 2021, **143**, 16428–16438.
111 H. Zhang, N. Liu, Y. Zhang, H. Cang, Z. Cai, Z. Huang and J. Li, *Colloids Surf., B*, 2024, **233**, 113665.

112 X. Niu, H. Yang, X. Wu, F. Huo, K. Ma and C. Yin, *Chem. Sci.*, 2024, **15**, 14924–14930.
113 Y. Dong, H. Wang, X. Zhang, Y. Ding, Y. Zou, J. Wang, S.-C. Zhao and Z. Li, *J. Nanobiotechnol.*, 2024, **22**, 481.
114 P. You, F. Lu, C. Ouyang, J. Yu, J. Gonzalez-Garcia, J. Song, W. Ni, J. Wang, C. Yin and C.-Q. Zhou, *ACS Appl. Mater. Interfaces*, 2024, **16**, 46066–46078.
115 H. Wang, Y. Wu, Y. Zhang, M. Zhou, S. Xu and Z. Li, *Optik*, 2021, **242**, 167325.
116 Y. He, Y. Wu, J. Mei, Y. Zhang, S. Xu and Z. Li, *Inorg. Chim. Acta*, 2022, **538**, 120994.
117 Y. Gambe, H. Kobayashi and I. Honma, *Chem. Eng. J.*, 2024, **479**, 147760.
118 C. Luo, Y. Zhu, Y. Xu, Y. Liu, T. Gao, J. Wang and C. Wang, *J. Power Sources*, 2014, **250**, 372–378.
119 Q. Zhao, J. Wang, Y. Lu, Y. Li, G. Liang and J. Chen, *Angew. Chem., Int. Ed.*, 2016, **55**, 12528–12532.
120 Y. Katsuyama, H. Kobayashi, K. Iwase, Y. Gambe and I. Honma, *Adv. Sci.*, 2022, **9**, 2200187.